6-1-2012

A Study of Histone Deacetylase Inhibitors: Determination of the Binding Energetics of Suberoylanilide Hydroxamic Acid with Zinc and Cobalt and Preliminary Screening of Nitric Oxide Donors

Erin Gallagher
erin.gall11@gmail.com

DePaul University
College of Science of Health: Chemistry Department

A Study of Histone Deacetylase Inhibitors: Determination of the Binding Energetics of Suberoylanilide Hydroxamic Acid with Zinc and Cobalt and Preliminary Screening of Nitric Oxide Donors

A Thesis in Biochemistry
by
Erin K. Gallagher

Submitted in Partial Fulfillment
of the Requirements
for the Degree of

Master of Science

June 2012

Acknowledgements

I wish to thank DePaul University for providing the funding for the experiments as well as the opportunity to complete my Masters degree. I would also like to thank my graduate advisors, Dr. Lihua Jin and Dr. Caitlin Karver for all of their support and guidance as well as Dr. Cathrine Southern for being a member of my thesis committee. Finally, I wish to thank Stephanie Lyngaas for helping in the data collection process which allowed me to complete this work.

Abstract

Inhibiting histone deacetylases (HDACs) can suppress tumor cell growth eventually leading to their death, making HDACs an important drug target. Therefore, understanding the mechanism behind inhibiting HDACs is imperative. To determine the thermodynamic parameters for the interaction of a known competitive HDAC inhibitor, suberoylanilide hydroxamic acid (SAHA), with zinc(II), the metal ion in the HDAC active site, and cobalt(II), isothermal titration calorimetry (ITC) was used. The results showed that SAHA binds to zinc(II) more strongly than it does to cobalt(II) as the equilibrium binding constants were $4.3 \pm 0.5 \times 10^2$ M^{-1} and $2.0 \pm 0.5 \times 10^2$ M^{-1} for zinc (II) and cobalt (II), respectively. In addition, the calculated value of $\Delta G°$ for SAHA and zinc(II) of -15.0 ± 0.3 kJ/mol compared to -35.6 kJ/mol for SAHA and HDAC suggest that the hydroxamic acid functional group contributes significantly to the overall binding energetics of the interaction. Additional titration experiments using the literature prototype for hydroxamic acid binding, acetohydroxamic acid (AHA), suggested that the binding parameters obtained for SAHA interacting with zinc(II) and cobalt(II) in the non-physiological mixture are likely comparable to what they would be in aqueous conditions. To further characterize HDAC as a drug target, various nitric oxide (NO) donors, known to chemically modify and inhibit HDACs, were screened using an HDAC8 discontinuous fluorogenic assay. These assays allowed the effectiveness of the NO donors to be determined through comparison of HDAC8 percent activity relative to a control. The screened commercially available NO donors displayed no inhibition, whereas SAHA, a different class of NO donor, did decrease HDAC8 activity. Overall these studies suggest that inhibitors which bind in the active site of HDACs are more effective than those that covalently modify cysteine residues.

Table of Contents

Chapter 1:
Introduction

1.1 Histone Deacetylases

Histone deacetylases (HDACs) remove an acetyl group from acetylated side chains of lysine residues in histones. The removal of the acetyl group results in positive charge density at the N-terminal region of histone proteins, and strengthens their interaction with negatively charged DNA, thereby blocking access of transcription factors and down regulating gene expression.[1] Figure 1.1 shows a schematic representation of the action of HDACs. In total, 18 HDAC isoforms have been discovered in humans and these are divided into four classes based on their structural similarity to yeast HDACs, cellular location, tissue specificity and enzymatic activity. Class I HDACs (1, 2, 3 and 8) are nuclear proteins that are ubiquitously expressed and act as co-repressors for nuclear receptors.[1] Class II HDACs (4, 5, 6, 7, 9, and 10) can shuttle between the nucleus and the cytoplasm in response to cellular signals. This class of HDACs is divided into two subclasses, class IIa (HDACs 4, 5, 7, and 9) and IIb (HDACs 6 and 10) where class IIb HDACs have two deacetylase domains compared to the single deacetylase domain found in class IIa. Class IV is composed of HDAC11 which is found in the nucleus and has a similar sequence to class I and II HDACs. Class III HDACs require an NAD^+ cofactor for their activity while all other classes are Zn^{2+}- dependent enzymes.[1]

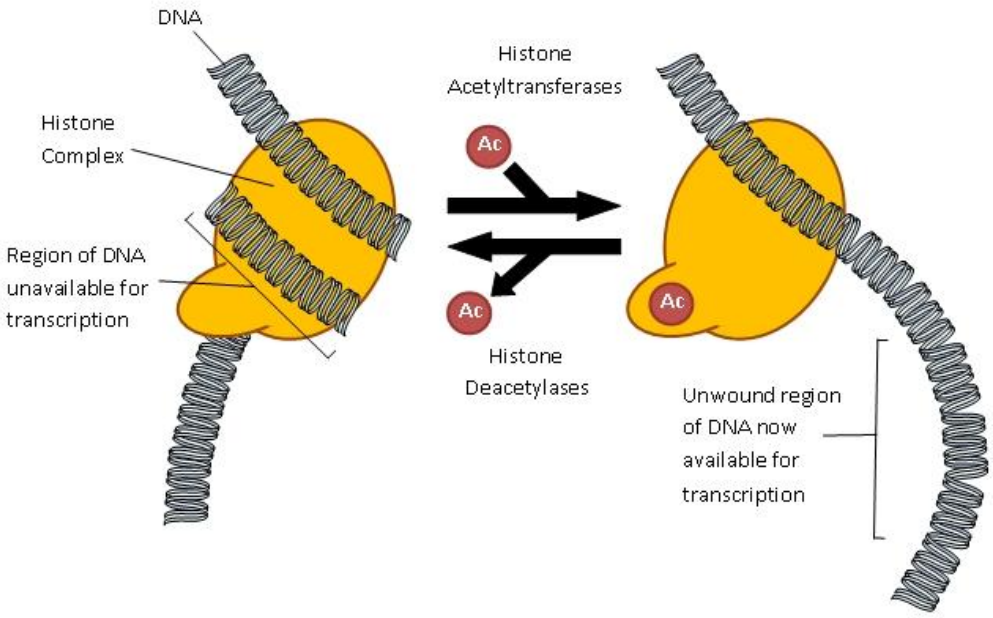

Figure 1.1: Action of histone deacetylases and histone acetyltransferases. *Histone acetyltransferases catalyze the transfer of acetyl groups to lysine residues on the histone protein to allow DNA to unwind and become available for transcription. Histone deacetylases catalyze the removal of acetyl groups to keep DNA tightly wound and unavailable for transcription. Taken on May 16, 2012 from http://www.di.uq.edu.au/proj6background*

Histones are small, positively charged nuclear proteins that associate with DNA in a specific stoichiometry to form a nucleosome. The DNA molecule winds around a core of eight histone proteins in a solenoidal supercoil to compact the DNA into a nucleosome. Once formed, the nucleosome assembles into chromosomes.[2] Figure 1.2 shows a generic representation of the histones and DNA interacting. This condensed form of DNA plays a major role in gene regulation by controlling transcription. Transcription is regulated by protein transcription factors that control target genes through interactions with specific regions of the DNA sequence or by inducing structural changes to DNA or histone proteins upon binding. Histones have a flexible tail in the N-terminal region that sticks out from the surface of the proteins. The tails of histone proteins are the main target for many post-translational modifications including acetylation, methylation, and phosphorylation.[3] Specifically, acetylation of histones is the source of

transcriptional activation by hyperacetylation, or transcriptional repression by hypoacetylation. The balance between activation and repression is largely controlled by histone acetyltransferases (HATs) and HDACs as shown schematically in Figure 1.1.[2]

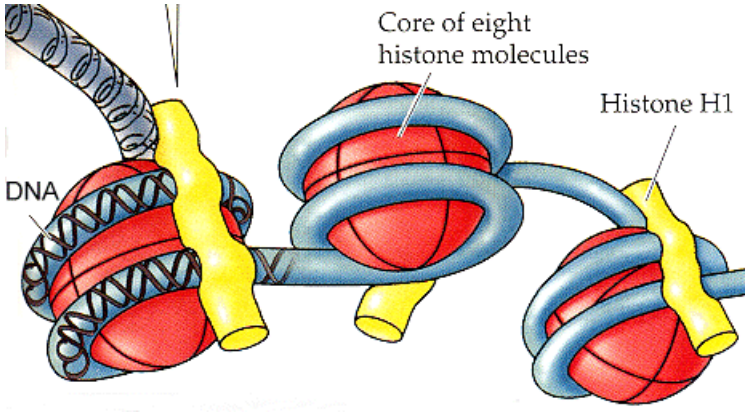

Figure 1.2: Structure of histone proteins. *DNA is wound around the histone proteins to form the condensed form of DNA known as chromatin. The action of HDACs is what signals the DNA to remain in the condensed state whereas the action of HATs loosens the DNA and makes it available for transcription. Taken on May 16, 2012 from* [*http://biology.kenyon.edu/courses/biol114/Chap01/chrom_struct.html*](http://biology.kenyon.edu/courses/biol114/Chap01/chrom_struct.html)

Most Zn^{2+}- dependent HDACs have highly conserved catalytic sites and function as multi-protein complexes.[4] Figure 1.3 shows the crystal structure of HDAC8. It contains a single domain, which has eight parallel β-sheets with the C-terminal ends of the β-strands creating large loops. Surrounding the β-sheets are eleven α-helices.[2]

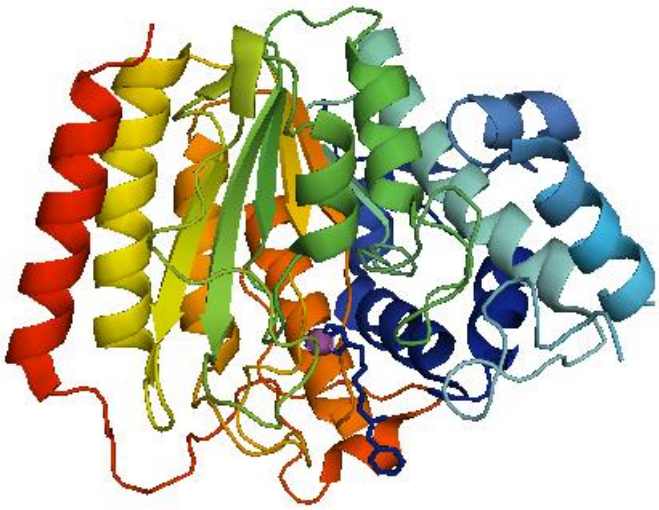

Figure 1.3: Crystal Structure of HDAC8 with bound inhibitor. *PDB structure 1T69 shows a single domain with 8 parallel β-sheets surrounded by eleven α- helices.*
Taken on May 30, 2012 from http://www.pdb.org/pdb/explore/explore.do?structureId=1T69

In the active site, a 12 Å long hydrophobic tunnel leads to the catalytic site containing zinc(II). During deacetylation, the tunnel is occupied by the four methylene groups of an acetylated lysine residue. At the bottom of the cavity is the Zn^{2+} ion, the essential component of the catalytic site.[1] Zinc(II) is penta-coordinated with three sites occupied by Asp178, His180 and Asp267; the other two sites are occupied by oxygen atoms, one from the acetyl group from the bound substrate and the other from a water molecule as shown in Figure 1.4 A and B.[1] Recently, a cavity has been discovered below the active site.[5] The cavity is formed from the loops that connect the β-strands. The walls of the cavity are mainly composed of glycine and other hydrophobic residues. One of the loops separates the cavity from the solvent and probably has some flexibility that allows the exchange of cavity contents with the solvent.[4] While the exact function of the cavity is unknown, it is an important consideration in inhibitor design because it is suspected to allow enough space for acetylated lysine residues to diffuse into the solvent through the cavity to make room for the inhibitor.[5]

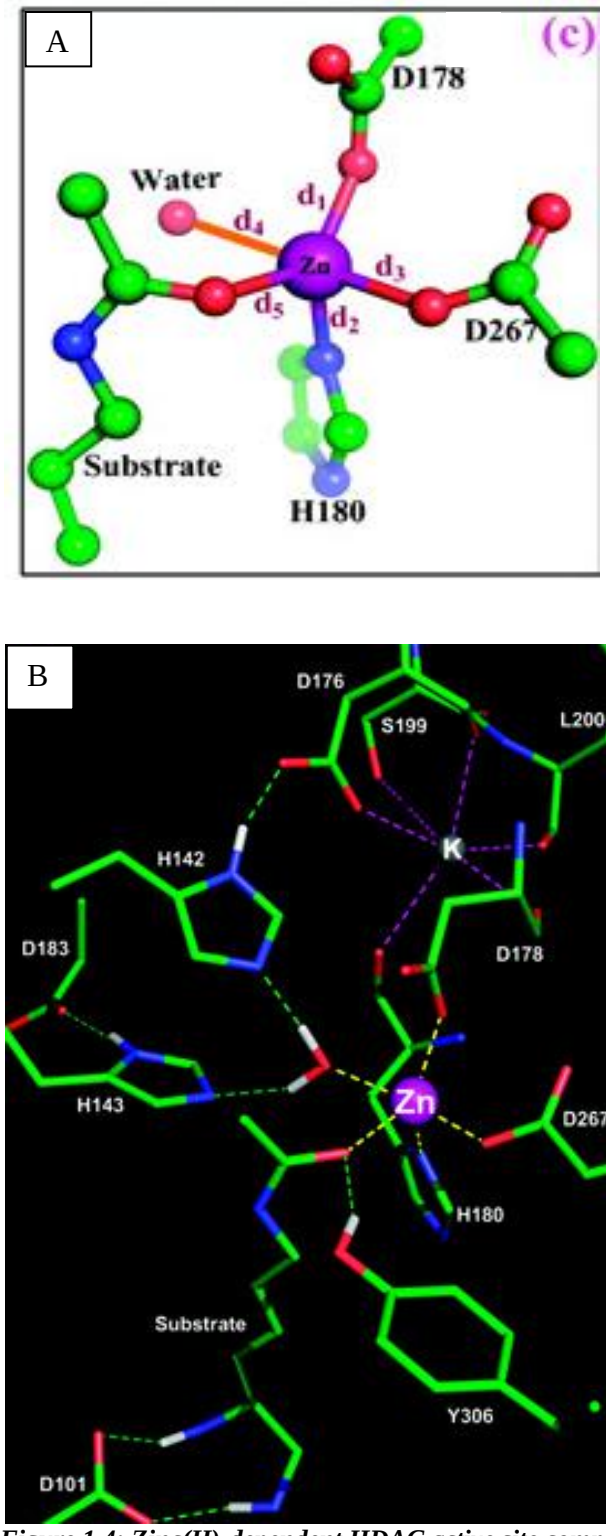

Figure 1.4: Zinc(II)-dependent HDAC active site components*. A. Zinc(II) coordination shell of HDAC8. B. Amino acid residues in HDAC8 active site surrounding the catalytic zinc(II). Important hydrogen bond interactions are shown with dashed green lines. Taken on June 1, 2011 from* https://wikis.nyu.edu/display/NYUHPC/Proton-Shuttle+Reaction+Mechanism+for+Histone+Deacetylase+8

1.2 Modes of Regulation of Histone Deacetylases

The ability of HDAC to deacetylate histone proteins that are part of the nucleosome requires them to be located in the nuclei of cells. However, class II HDACs are also found in the cytoplasm, implying that they can shuttle between the nucleus and cytoplasm of cells.[6] In the cytoplasm, HDACs are unable to make an impact on transcription directly since they are not in close proximity to the histone proteins they affect. Because of this, cytoplasmic HDACs are unable to deacetylate histones given that their intended substrate is not available.[6] Thus, the proper distribution of HDACs in the nucleus and in the cytoplasm is critical for the correct regulation of transcription.[6] Thus, the sub cellular localization of HDACs is a highly regulated pathway that uses a diverse set of mechanisms.

The sub cellular location of HDACs can be regulated by the nuclear localization sequence (NLS) and the nuclear export signal (NES) which shuttle HDACs through nuclear pores. Additionally, phosphorylation of binding sites on the regulatory protein 14-3-3 dictates HDAC localization. Inhibition of HDAC 14-3-3 site phosphorylation results in nuclear accumulation of HDACs and transcriptional activation while activation of phosphorylation leads to cytoplasmic accumulation and transcriptional inhibition.[6] There are four broad types of HDAC kinases that participate in this regulatory pathway. The first class of kinases shown to regulate class IIa HDAC localization is the Ca^{2+}/calmodulin-dependant kinase (CaMK) family. This class of kinases has been shown to stimulate the disassembly of the HDAC4 complex with myocyte enhancer factor 2 (MEF2) leading to cytoplasmic accumulation of HDAC4.[7] Another type of kinase, protein kinase D (PKD), has been shown to directly phosphorylate four serine residues leading to nuclear export of HDAC7.[8] Two members of the microtubule affinity-regulating kinase (MARK)/Par-1 family (MARK2 and MARK3) phosphorylate a sequence which is similar

to the signaling sites in Class II HDACs.[9] Finally, the newest HDAC kinase family, AMP-activated protein kinase/sucrose nonfermenting 1-like kinases (AMPK/SNF1), can use salt-inducible kinase (SIK1) to phosphorylate two 14-3-3 binding sites of HDAC5.[10] The existence of multiple families of kinases targeting class II HDACs suggests that the biological roles of these transcriptional repressors are plentiful.

The phosphorylation-dependent regulation of HDACs is a reversible process and thus, dephosphorylation via protein phosphatases, specifically PP1 and PP2A, would be expected to relocalize HDACs in the nucleus and activate their transcriptional abilities.[6] This is exemplified by calyculin A, which is an inhibitor of PP1 and PP2A. In the presence of this inhibitor, HDAC4 is located in the cytoplasm of cells which implicates PP1 and PP2A play a critical in the mechanism of HDAC4 localization.[11] Overall, cellular kinases and phosphatases regulate different signaling pathways allowing for diverse control of HDAC localization and thereby function.

1.3 Inhibition of HDACs

The precise regulation of HDACs in response to different cellular signals is essential for proper post-translational modifications of histones. Histone deacetylases are typically over expressed in tumor cells and in oncoproteins.[12] Oncoproteins typically use this increased concentration of HDACs to escape the apoptotic pathways and cause cells to proliferate, leading to cancer. Thus, inhibiting HDACs can induce a variety of genes leading to multiple mechanisms of tumor cell death through apoptosis; this makes them a promising approach for the treatment of cancer.[13]

Many types of HDAC inhibitors (HDAC*i*'s) are available today including short chain fatty acids, hydroxamic acids, cyclic tetrapeptides, aliphatic acids and benzamides. Suberoylanilide hydroxamic acid (SAHA) and Trichostatin A (TSA) are both hydroxamic acids and are the most well studied HDAC inhibitors.[12] As shown in Figure 1.5, most HDAC inhibitors consist of three structural components: a zinc(II) binding group (ZBG) that chelates zinc(II) at the active site; a linker region, which in the case of SAHA is six carbons long and sits in the hydrophobic tunnel leading to the active site; and a cap which is typically an aromatic moiety that interacts with residues on the surface of HDAC enzymes. These structural components are responsible for inhibition of HDACs and thus suppression of tumor cell growth.[14]

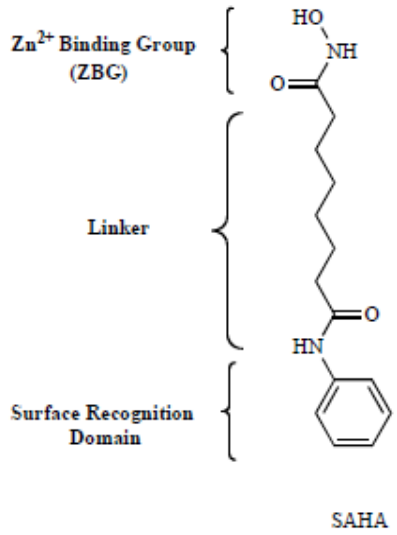

Figure 1.5: General Structure of HDAC Inhibitor. *The general parts that make up an HDAC inhibitor, using the structure of SAHA as an example.*[1]

There are numerous pathways through which class I, II and IV HDAC*i*'s can mediate cell death. They can terminate the cell cycle at either G1 or G2/M causing tumor cell death. Histone deacetylase inhibitors affect the DNA damage and repair pathway by generating DNA double stranded breaks to elicit a DNA damage response leading to apoptosis.[12] They affect mitosis by targeting microtubules and impairing control of mitotic progression. They can induce apoptosis

directly through the extrinsic (activation of death receptors and ligands) or intrinsic (mitochondrial disruption) pathways. They have an anti-angiogenic effect which stops the production of new blood vessels, forcing tumor cells to die.[12] The inhibitors affect the misfolded protein response (MPR) pathway by generating stress to create a response. If the stressor does not subside apoptosis will occur. Histone deacetylase inhibitors also induce autophagy in cancer cells causing cell death by self digestion of cellular components.[12] These mechanisms, which ultimately lead to apoptosis, are all mediated via HDAC inhibitors.

1.4 Suberoylanilide Hydroxamic Acid (SAHA)

Suberoylanilide hydroxamic acid is currently an FDA approved drug called Vorinostat (produced by Merck) that has potency in the nanomolar range and is used for the treatment of Cutaneous T-cell lymphoma. It is also in various phases of clinical trials for other types of cancers including breast, ovarian, lung, and blood, to name a few.[15] Suberoylanilide hydroxamic acid binds to HDAC and inhibits by inserting its linker into the hydrophobic tunnel and making contacts with multiple amino acids. The zinc(II) binding hydroxamic acid group reaches the bottom of the tunnel and coordinates to zinc(II) through its carbonyl and hydroxyl oxygen's to create a penta-coordinated ion.[5] The zinc(II) binding group (ZBG) also hydrogen bonds with nearby histidine and tyrosine residues and replaces water in the active site with its hydroxyl group. Finally, the aromatic moiety "caps" the opening to the tunnel by interacting with surface residues as seen in Figure 1.4, 1.5, and 1.6.[5] Suberoylanilide hydroxamic acid binds very strongly to zinc(II) and the amino acids in the active site with a K_d of 0.58 ± 0.14 μM that was determined by a fluorescence assay with coumarin labeled SAHA and HDAC.[16]

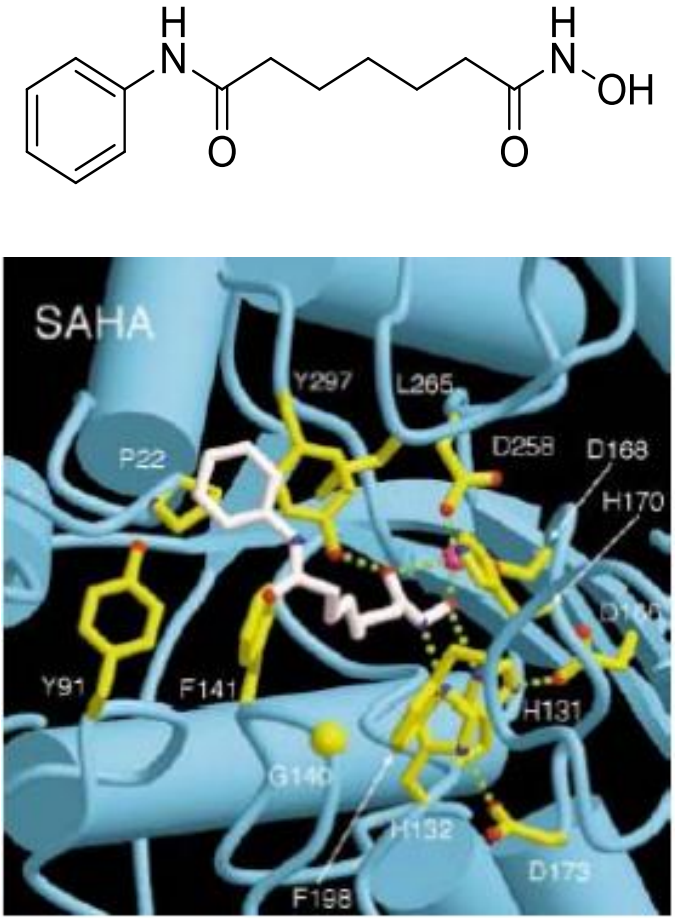

Figure 1.6: Skeletal and Crystal structure of SAHA. *Interaction of a known HDAC inhibitor, SAHA, with active site residues of a HDAC homologue known as HDLP.*[4]

1.5 Isothermal Titration Calorimetry

Isothermal titration calorimetry (ITC) is an efficient analytical method to determine the thermodynamic parameters for a given interaction and can be applied over a broad range of systems. Isothermal titration calorimetry works by measuring the heat produced during a titration reaction. Upon titration of one reactant (titrant) into the sample cell containing the other reactant (titrate), the difference in heat between the thermocoupled reference cell and the sample cell is measured. Heat is either released to yield an exothermic reaction or absorbed to yield an endothermic reaction.[17] The heat of reaction is measured through the amount of power required

to maintain a difference in temperature between the reference and sample cells equal to zero. With subsequent additions of titrant, the heat signal diminishes, indicating that binding is near completion. The concentrations of titrant and titrate are chosen so that only a portion of titrant binds upon each titration.[18] This makes the final binding curve of heat generated per injection versus titrant: titrate molar ratio dependent on the affinity of the interaction, stoichiometry, and enthalpy change.

A c-value defined as the products of stoichiometry (n), equilibrium binding constant (K_a) and concentration of titrate, c= (n)(K_a)([cell], is used to determine the appropriate range of concentrations to be used in a titration experiment.[18] An acceptable range of c-values should be between 1-1000 or even better, 5-500. This ensures that the resulting binding isotherm has a unique shape that allows for the extraction of a one set of binding parameters. Figure 1.7 shows an ideal titration curve that has a unique shape. Additionally, it is important to note that to shift binding to completion, the titrant concentration is chosen to be at least 10 times the titrate concentration.[18]

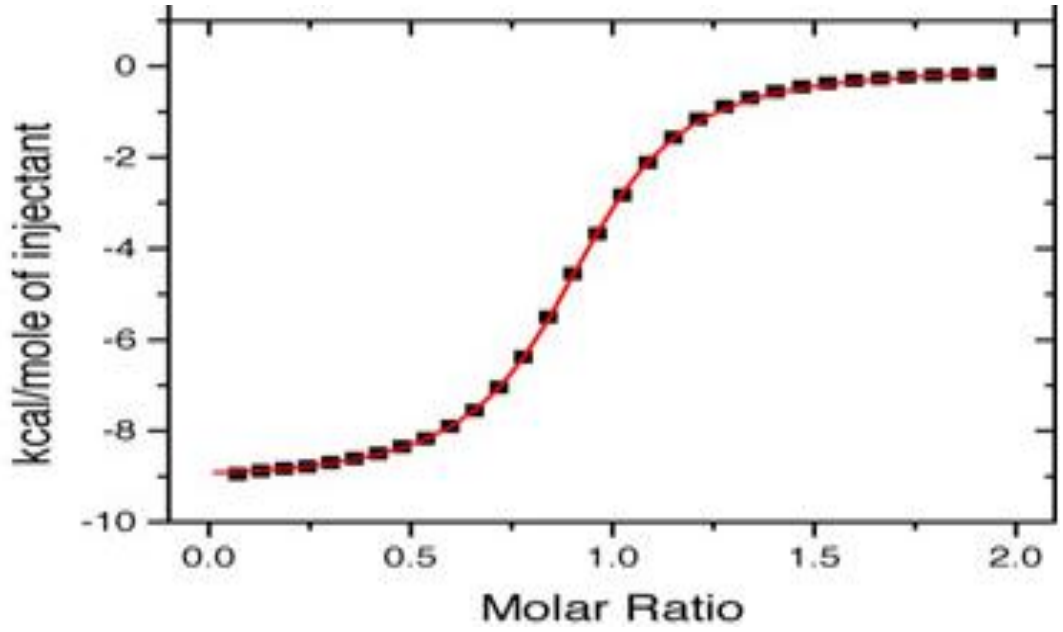

Figure 1.7: Ideal shape of a binding isotherm. *An S-shaped curve is the ideal shape of a binding isotherm. It is a unique curve that only fits one set of parameters.*

By integrating the heats of each injection, a binding curve can be constructed. The heat generated or absorbed, Q, during the binding interaction is directly related to the fraction of ligand bound (Equation 1).[19,19b] The derivation of the equation for the fraction of ligand bound is shown below. After correcting for volume displacement effects, the resulting isotherm is fit using an iterative, one set of identical sites model, (Equations 2 and 3) in the Origin 7.0 software to determine the thermodynamic parameters.[19b] Equations 2 and 3 are mathematically equivalent, but Equation 3 uses terms that are known, such as total ligand and metal concentration, whereas Equation 2 includes the free ligand concentration, which is difficult to calculate. This heat represents the change in enthalpy (ΔH) for the interaction. Because the binding is determined via titration, the stoichiometry (n) and equilibrium binding constant (K_a) can also be determined.[9,19b] Once these parameters have been determined, the actual concentrations of free ligand, free metal and the ligand-metal complex can be calculated allowing ΔG to be determined from $\Delta G°$ using Equation 4.[19a] From the values of ΔH and ΔG, the Gibb's free energy equation (Equation 5) can

be used to calculate the value of ΔS.[19a] However, for our studies, the ΔG° was calculated using Equation 6.

$$[LM] \leftrightarrow [L] + [M]$$

$$K_d = \frac{[L][M]}{[LM]}$$

$$fraction = \frac{[LM]}{[LM] + [M]}$$

$$[L][M] = K_d[LM]$$

$$fraction = \frac{\frac{[L][M]}{K_d}}{\left(\frac{[L][M]}{K_d}\right) + [M]}$$

$$fraction\ of\ ligand\ bound = \frac{[L]K_a}{([L]K_a) + 1} \qquad (1)$$

$$Q = V_o([LM] + [M])\Sigma \left[\frac{n_i \Delta H_i K_{ai}[L]}{([L]K_a) + 1}\right] \qquad (2)$$

$$Q = \frac{n([LM]+[M])\Delta HV_0}{2}\left[1 + \frac{([LM]+[L])}{n([LM]+[M])} + \frac{1}{nK([LM]+[M])} - \sqrt{\left(1 + \frac{([LM]+[L])}{n([LM]+[M])} + \frac{1}{nK([LM]+[M])}\right)^2 - \frac{4([LM]+[L])}{n([LM]+[M])}}\right] \qquad (3)$$

$$\Delta G = \Delta G° + RTlnQ \qquad (4)$$

$$\Delta G = \Delta H - T\Delta S \qquad (5)$$

$$\Delta G° = -RTlnK \qquad (6)$$

In general, for an inhibitor to be an effective drug candidate with minimal toxicity, it needs to possess an optimal affinity for the target enzyme but minimal affinity for other proteins in the cell. To accomplish this, it is necessary to determine the specific contribution of different functional groups of the inhibitor in order to fine tune affinity.

To better understand the interaction of SAHA with HDAC and thus its ability as an inhibitor, a comprehensive look at the energetic contribution of each of the three regions of SAHA was examined. In particular, the contribution of zinc(II) chelation to the overall interaction of SAHA with the active site was determined. To do this we examined the binding energetics of free zinc(II) to SAHA using isothermal titration calorimetry. The nonpolar nature of the major portion of SAHA predicts that it is water insoluble, making it impossible to characterize the interaction in a buffer. We therefore turned to a mixture containing 60% methanol and 40% N-ethylmorpholine (NEM) buffer at pH 6.80. The binding of zinc(II) to acetohydroxamic acid (AHA), which is analog of SAHA without the linker and cap regions, was also examined in the methanol:buffer mixture as well as NEM buffer to assess the effect, if any, the solvent has on the binding parameters.

Studies have suggested that *in vitro* replacement of zinc(II) in the active site of HDAC with cobalt(II) allows the enzyme to retain the highest amount of activity, compared to replacement using other transition metals such as iron(II) and nickel(II).[20] This prompted the use of cobalt(II) as the alternative transition metal ion in our ITC studies with SAHA and AHA. Cobalt(II) was used to compare the binding parameters obtained, specifically affinity and $\Delta G°$, to those obtained from studies of SAHA and AHA binding to zinc(II). The same experiments carried out for zinc(II) binding to SAHA and AHA in under both solvent conditions were also

performed using cobalt(II). In all cases, stoichiometry (n), binding affinity (K_a) thus standard Gibb's free energy change ($\Delta G°$), enthalpy change (ΔH) and entropy change (ΔS) were reported.

From these studies we wish to gain a greater knowledge of how SAHA interacts with different metal ions, specifically zinc(II). Using affinity data, conclusions can be made about whether or not metal ion binding is a critical component for binding strength and thus an important component of inhibitor design. Studying the binding interaction of SAHA and AHA with zinc(II) and cobalt(II) will allow for greater insight into the stoichiometry of binding, the strength of binding, and the overall binding energetics of the interaction. These parameters will provide previously unavailable data to those studying SAHA for its anti-cancer abilities and possible ways to design stronger inhibitors.

1.6 Nitric Oxide as an Endogenous Signaling Molecule

Nitric oxide (NO) is a small, potentially toxic, free radical byproduct of cellular metabolism that plays an important role in numerous cellular functions. The most important chemical property of NO that facilitates its role as a signaling molecule is that it is neutral, allowing it to easily diffuse across cellular membranes. Nitric oxide is produced *in vivo* from L-arginine through the action of nitric oxide synthase (NOS).[21] Nitric oxide synthases have three isoforms: neuronal NOS (nNOS), endothelial NOS (eNOS) and inducible NOS (iNOS). Neuronal and endothelial NOS are expressed continuously while iNOS is expressed through stimulation of various inflammatory agents such as cytokines and endotoxins, thereby inducing inflammation.[22] This inflammation helps kill or slow the growth of invading organisms. Inducible NOS is regulated through the availability of calmodulin, L-arginine, NADPH and tetrahydrobiopterin. Interestingly, iNOS produces the greatest amount of NO; this ability is

associated with a number of tumor pathologies.[23] The effectiveness of nitric oxide produced by iNOS on tumors seems to be dependent on iNOS activity, distribution, concentration, duration of exposure to NO and the cell's sensitivity to NO. Without the cooperation of existing blood vessel networks, which is largely regulated by NO, tumors cannot metastasize.[23] Not surprisingly, once these small inflammatory molecules are produced they play a critical role in the cell signaling pathways in the cardiovascular system, in neurons and in the immune system.[21]

The mechanisms of NO signaling through covalent modification of amino acid residues are plentiful and can be placed into three main categories, including: the S-nitrosylation of thiol groups, the formation of peroxynitrite ($ONOO^-$) which leads to nitrotyrosine formation, and the donation of electrons to transition metal ions, usually copper(II), zinc(II) and iron(II), thereby altering the activity of the target enzymes.[24] Nitrosylation and nitrotyrosine formation occur when NO levels are high (>1 μM) whereas electron transfer with transition metals occurs at lower concentrations (<1 μM). The pathway that nitric oxide takes to begin a signaling cascade depends on the local and surrounding environment concentration of NO. Once synthesized, NO diffuses out of the cell and can act locally to affect nearby cells. Its action is restricted to local effects because NO is highly unstable. [24]

The ability of nitric oxide to inhibit HDACs is an emerging interest in the medical community because of its potential use for the treatment of neoplasia, several types of cancers and autoimmune diseases such as rheumatoid arthritis and systematic lupus erythematosus.[25] There is increasing evidence that nitric oxide acts by covalently modifying cysteine residues in target proteins, such as HDAC8. Cysteine nitrosylation (S-nitrosylation) is a selective and specific signal controlled by cellular nitric oxide. S-nitrosylation of transcription factors, such as histone deacetylases, is one way that NO can regulate gene expression.[26] S-nitrosylation

regulates the interaction of transcription factors with chromatin by acetylating or deacetylating chromatin that is associated with gene promoter regions. Altering the acetylation state of chromatin is accomplished through the action of HATs and HDACs on the gene promoter regions of chromatin. Therefore, nitric oxide plays a role in the recruitment of HDACs to the proper regions of chromatin that require modifications.

1.7 Nitric Oxide as an Exogenous Signaling Molecule

The use of nitric oxide donors as exogenous signaling molecules was introduced more than a century ago through the use of vasodilators. To better understand the involvement of NO in a biological system, two approaches can be taken.[27] The first is to inhibit NO synthases to prevent endogenous formation of nitric oxide and the second is to administer exogenous NO. The use of exogenous NO is difficult because the delivery of nitric oxide gas is complicated. However, to circumvent this problem compounds that release NO in a controlled manner have been utilized. These compounds are referred to as "NO-donors". The action of these exogenous NO donors mimics an endogenous NO response to act on a multitude of pathways.[27]

Because of their unique properties, the potential uses of nitric oxide donors are broad. There are four main types of direct nitric oxide donors: diazeniumdiolates (NONOates), heterocyclic NO donors, S-nitrosothiols and S-nitrosylated sugars. Diazeniumdiolates mainly release NO through spontaneous chemical decomposition; this process is pH and temperature dependent. The most common NONOates are diethylamine (DEA) NONOate and diethylenetriamine (DETA) NONOate. The structures of these compounds are shown in Figure 1.8. The majority of research with these compounds is based in studying cardiac health and blood vessel dilation.[28] Another type of diazeniumdiolate is O(2)-(2,4-dinitrophenyl) 1-[(4-

ethoxycarbonyl)piperazin-1-yl]diazen-1-ium-1,2-diolate or JS-K whose structure is also shown in Figure 1.8. This compound is a potent anti-cancer agent, specifically for leukemia that is currently in clinical trials. [29]

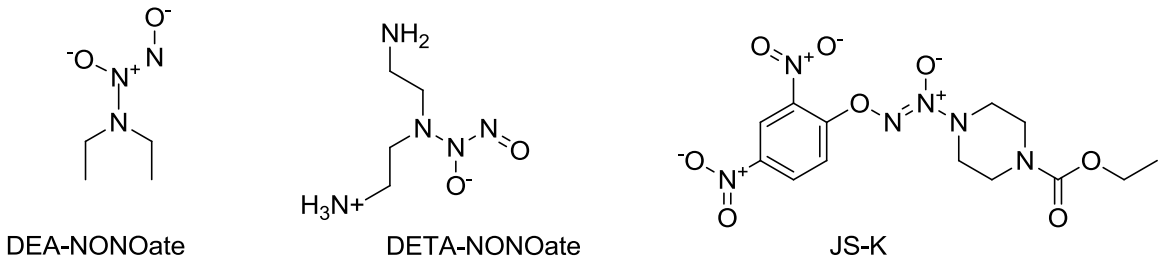

Figure 1.8: Structures of Common Diazeniumdiolates.

Heterocyclic NO donors differ from other types of NO donors because they require cofactors such as molecular oxygen or thiols to facilitate the release of NO.[28] While little is known about this class of compounds they have been shown to acts as vasodilators and to play a role in platelet adhesion as well as preventing thrombosis. The most common examples of heterocyclic NO donors are molsidomine, SIN-1 and Linsidomine. Figure 1.9 shows the structures of these three compounds.

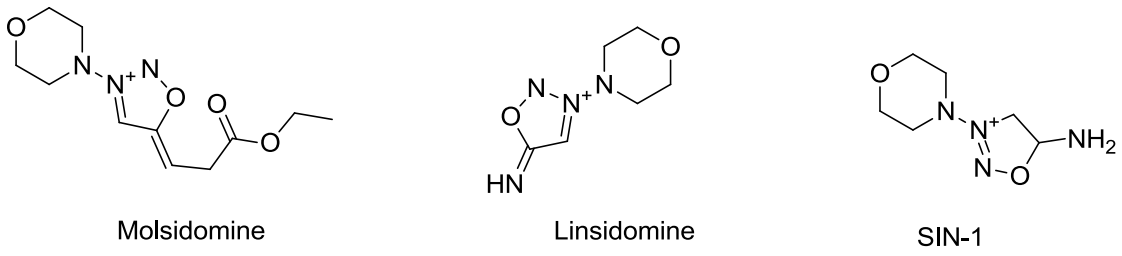

Figure 1.9: Structures of Common Heterocyclic NO donors.

S-nitrosothiols, another class of NO donors, includes S-nitroso-N-acetylpenacilamine (SNAP) and S-nitrosocysteine (L-CysNO). The structures of SNAP and L-CysNO are shown in Figure 1.10. This class of compounds is the most advantageous because they do not induce

oxidative stress, are naturally occurring and spontaneously release NO.[28] These compounds are involved in the upkeep of cardiac muscle and inhibition of platelet aggregation.[28] In cancer, they have been shown to modify tumor blood flow and brain permeability of tumors.[30]

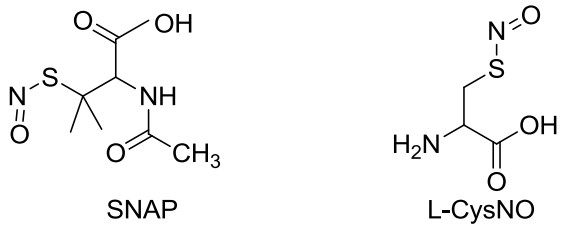

Figure 1.10: Common S-nitrosothiols.

The final type of nitric oxide donors are S-nitrosylated sugars. They are a type of thiol sugar that generate NO spontaneously. S-nitroslyated sugars are used to treat decreased skin blood flow due to decreased vasodilatation.[28] This group of NO donors is the least studied due to problems when the drug is administered orally such as significant and prolonged headaches and extreme fatigue.[31] The most common and widely used version of this class is S-nitroso-1-thio-2,3,4,6-tetra-*O*-acetyl-β-D-glucopyranose or D-SNAG whose structure is shown in Figure 1.11.[28]

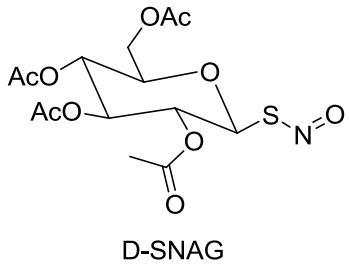

Figure 1.11: Structure of D-SNAG thiol sugar.

In addition to the general classes of NO donors, additional types of NO donors exist. In this study, ethanesulfohydroxamic acid (ESHA) was also tested as potential nitric oxide donor. From Figure 1.12, it is evident that ESHA has a very similar structure to that of SAHA and AHA sharing similar binding groups of a sulfonyl hydroxamic acid compared to a hydroxamic acid. This compound acts as a dual NO and HNO donor to inhibit enzymes.[32] Sodium nitroprusside, shown in Figure 1.13, is potent and releases NO spontaneously in the form of a nitrosyl group bound to iron. This compound is used for treatment of hypertension and heart failure.[28]

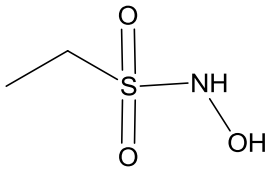

ESHA

Figure 1.12: Structure of Ethanesulfohydroxamic acid.

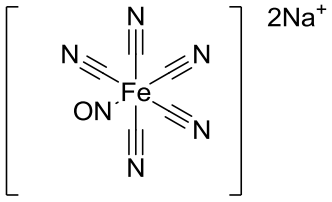

SNP

Figure 1.13: Structure of Sodium nitroprusside.

The uses of nitric oxide donors clinically as small molecule drugs are plentiful. The most studied actions of NO are in the cardiovascular system where it increases vasodilatation. Other uses of NO donors are their effects on the immune system to decrease cell proliferation, platelet aggregation and platelet adhesion. Additionally, NO donors have been shown to increase apoptosis and decrease cytokine release and they are also used for pain relief. [28]

Organic nitrates are the most common kind of NO donor drug; with glyceryl trinitrate, GTN (nitroglycerin) and isosorbide mononitrate (ISMN) being the most common. Both GTN

and ISMN are used for pain relief and to treat heat attacks (nitroglycerin).[33] The chemical structures of both GTN and ISMN are shown in Figure 1.14. Another NO donor that is currently used is SNP, which provides rapid lowering of blood pressure which is used for patients with hypertension. It is also considered the gold standard for vasodilators. The chemical structure of SNP is shown in Figure 1.13. Currently no NONOates are being used clinically although DEA-NONOate and DETA-NONOate are heavily studied for possible treatments of hypertension, lung injuries, erectile dysfunction, and thrombosis.[28] Interestingly, NONOates have been receiving interest as a possible mode to deliver high concentrations of NO specifically to tumor cells.[33] JS-K, another NONOate, slows the growth of a wide range of cancer cells without harming healthy cells and is in clinical trials for treatment of leukemia.[29]

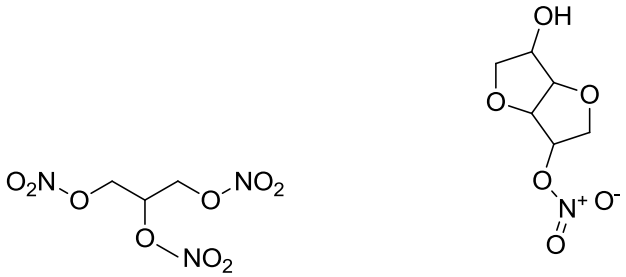

GTN ISMN

Figure 1.14: Chemical Structures of GTN and ISMN.

S-nitrosothiols are more tissue specific than other types of NO donors and are also potent anti-platelet drugs that inhibit aggregation.[33]. S-nitroso-N-acetylpenicillamine (SNAP) has been shown to be useful in improving coronary endothelial function. S-nitroso-glutathione (GSNO) is used for selective treatment of arterial disorders, as opposed to treating both arteries and veins. It has also been shown to decrease the occurrence of cerebral embolisms, and to have neuroprotective properties by regulating the antioxidant and apoptotic pathways.

Nitric oxide donors also act as inhibitors of HDACs. The NO donors are hypothesized to interact with three cysteine residues on the HDAC surface (not in close proximity the active site)

to render it inactive. Current studies have used GSNO as an exogenous NO donor to inhibit HDACs.[34] Interestingly, both SAHA and TSA release nitric oxide upon oxidation in the body and have been shown to not only inhibit HDACs by interacting with the active site but to also release NO that interacts with the protein surface.[35] Nitric oxide acts on both nuclear and cytoplasmic HDACs and preliminary studies suggest that NO may prevent HDACs from assembling the necessary multi-protein complexes for its activity.[34]

1.8 Fluorogenic Inhibition Assay

Enzyme assays are an analytical tool that determines an enzyme's activity over time or at an endpoint. Enzyme assays play a critical role in the drug discovery process by determining if inhibition is taking place or if the enzyme activity has increased.[36] One such assay that releases a fluorescent product upon reaction is called a fluorogenic assay. In general, this technique uses a substrate that has fluorogenic properties that change in proportion to the rate of cleavage from the enzyme. For proteolytic enzyme reactions, a fluorophore is adjacent to the site of proteolytic cleavage which in turn produces fluorescence. The fluorescent signal is directly proportional to the amount of substrate cleaved.[37]

Specifically in the case of HDAC8, the assay most commonly used is a discontinuous coupled assay. The peptide substrate containing an acetylated lysine and a quenched fluorophore is deacetylated by HDAC8. After deacetylation, a developer solution containing a protease cleaves the peptide further which causes the release of the fluorophore. A general reaction scheme for this process is shown in Figure 1.15. While many types of fluorogenic substrates are available, we used 4-acetyl-L-Arg-L-His-L-Lys(ε-acetyl)-L-Lys(ε-acetyl)-coumarin (Fluor de Lys Substrate) for the assay. This particular type of assay is a discontinuous endpoint assay, meaning that the fluorescence is not measured over time but rather at the endpoint of consecutive

reactions of HDAC8 followed by the protease in the developer solution. Based on the relative fluorescent units (RFUs) obtained for a particular reaction with inhibitor present compared to a control without inhibitor, it can be determined whether or not the enzyme is being affected. A decrease in RFUs indicates inhibition while an increase in RFUs points towards activation. These data are typically presented as percent activity, with the control serving as 100% activity.

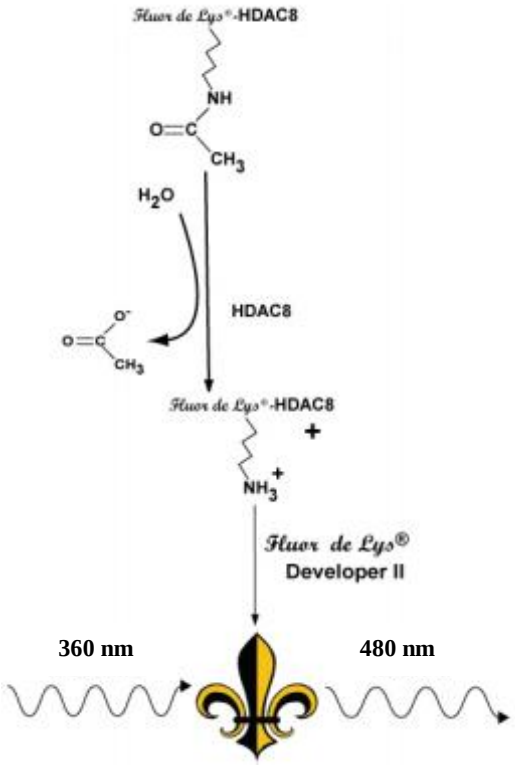

Figure 1.15: Reaction scheme of the HDAC8 Fluorimetric Activity Assay. *Substrate is deacetylated by HDAC8and developer produces a fluorophore that is read at an excitation wavelength of 360nm and a emission wavelength of 480 nm.*[38]

While the exact mechanism is unknown, nitric oxide plays a role in the regulation of inflammatory pathways and in inflammatory cancers. Thus, this study was conducted to determine if HDACs are inhibited by nitric oxide donors. The information gathered here will be used to begin to understand the modes of HDAC inhibition and regulation through nitric oxide

donors and potential drug targets for inflammatory cancers. To begin, we used a broad range concentration screening technique to determine whether or not HDAC8 is inhibited at high and low concentrations of SNP, SNAP, JS-K, DEA-NONOate, DETA-NONOate and L-CysNO. The NO donors that showed inhibitory properties were further tested using a tighter range of concentrations to try to determine the IC_{50}. The IC_{50} or half maximal (50%) inhibitory concentration (IC) is a measure of the overall effectiveness of an inhibitor. The IC_{50} provides critical information on the potency of the inhibitor as well as information that is useful when determining the dosage of the drug candidate. Additional screens were performed using AHA, SAHA and ESHA to test their ability as inhibitors.

Chapter 2: Isothermal Titration Calorimetric Studies of SAHA and AHA Binding to Zn^{2+} and Co^{2+}

The interaction of SAHA and AHA with the transition metals zinc(II) and cobalt(II) were studied using ITC. From the resulting data, the binding parameters including the stoichiometry of binding (n), the equilibrium binding constant (K_a), the change in entropy (ΔS), the change in enthalpy (ΔH) and the standard change Gibb's free energy ($\Delta G°$) were determined. All the parameters were obtained at 25°C and at a pH of 6.80. The buffer used was an NEM buffer consisting of 50 mM NEM and 150 mM NaCl.

Suberoylanilide hydroxamic acid and AHA were titrated with zinc(II) and cobalt(II) to yield the thermodynamic binding parameters for each system. Zinc(II) was chosen because it is found at the active site of HDAC *in vivo*. Cobalt(II) was used because when zinc(II) in the active site of HDAC8 is replaced with cobalt(II) *in vitro* the enzyme still retains its activity allowing for an interesting point of comparison between the binding parameters.[20]

Suberoylanilide hydroxamic acid is insoluble in aqueous media but soluble in methanol.[39] Titrations were therefore first carried out in anhydrous methanol. However, the data were not reproducible. Upon investigation it was determined that small, but possibly varying amounts of water were likely present in the methanol and in the $ZnCl_2$ and $CoCl_2$ solutions of metal ions. The variations in the ITC data obtained in methanol are likely a result of heats related to solvation and desolvation, which varies across solvent conditions.

To counteract this problem, anhydrous methanol was aliquoted under nitrogen atmosphere. This resulted in smaller heats of binding but still unsatisfactory reproducibility. Finally, a mixture of methanol and buffer, was used to eliminate the interference of water in the solvent while still ensuring sufficient SAHA solubility. Specifically, a mixture of 60% anhydrous methanol and 40% NEM buffer at pH 6.80 was found be suitable as it yielded reproducible results as long as the samples were not degassed. Degassing is a process where trapped air bubbles are removed from the solvent under a vacuum. Due to the volatile nature of methanol, degassing alters the methanol:buffer mixture composition and also the solute concentration, making data not reproducible. Therefore samples containing methanol were not degassed.

2.1 SAHA- Zn^{2+} Binding in the Methanol: Buffer Mixture

The binding interaction of SAHA and zinc(II) was determined in the above mixture with 10 mM SAHA being titrated into 1 mM zinc(II). Figure 2.1 shows raw data and the resulting binding isotherm for a sample SAHA into zinc(II) titration experiment. Figure 2.2 shows an overlay of the isotherms of three triplicate experiments. On the same figure, an isotherm of zinc(II) ion into the methanol:buffer mixture control experiment is shown. A constant corresponding to the plateau value (the constant where the binding isotherm is at its flattest) of the resulting isotherm was subtracted as well.

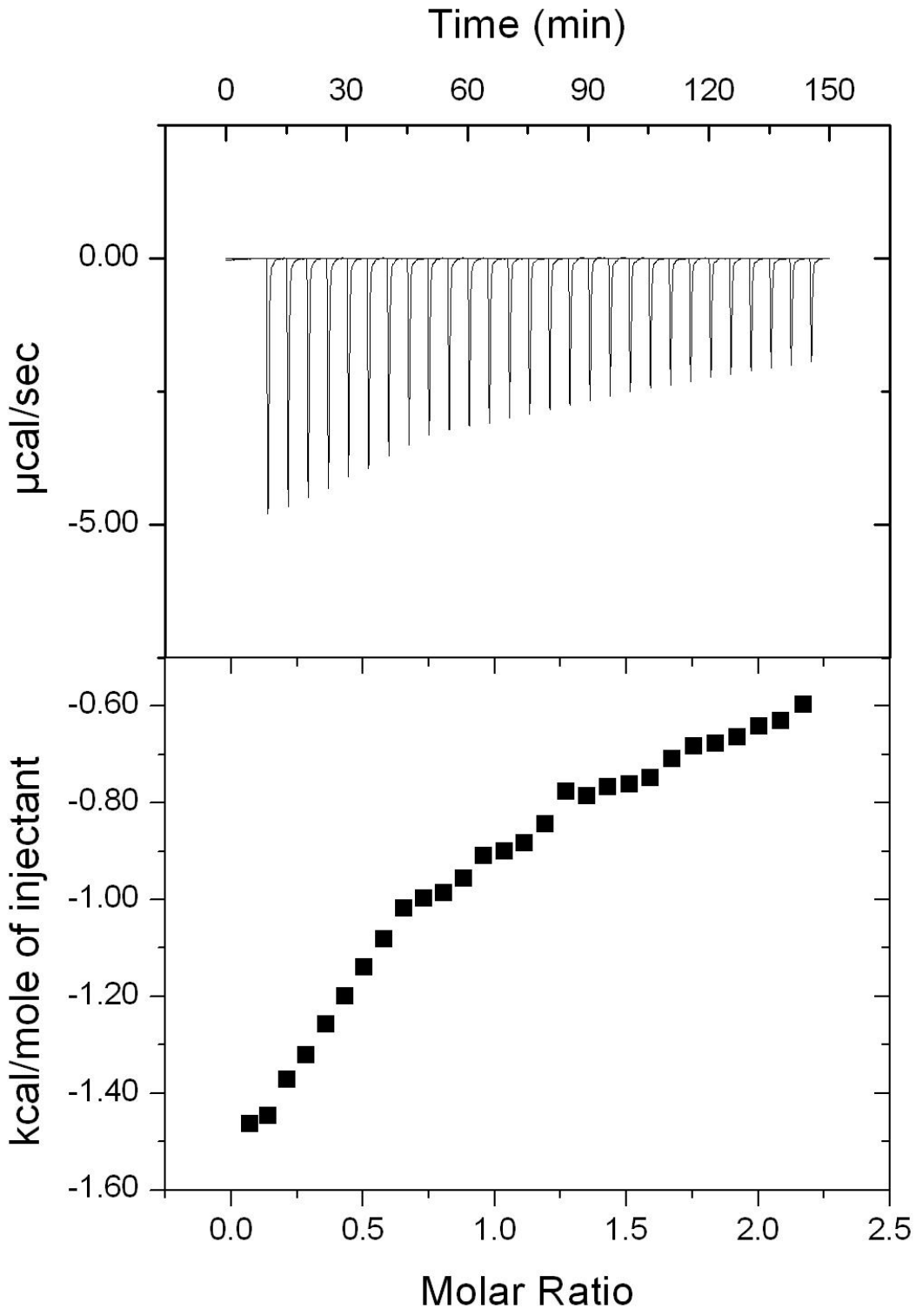

Figure 2.1: Titration calorimetry of SAHA into zinc(II). *A 10 mM solution of SAHA was titrated at 25°C, using injections of 10 µL, into a 1 mM solution of* $ZnCl_2$. *Both were prepared in 60% anhydrous methanol and 40% buffer containing 50 mM NEM, 150 mM NaCl, pH 6.80.*

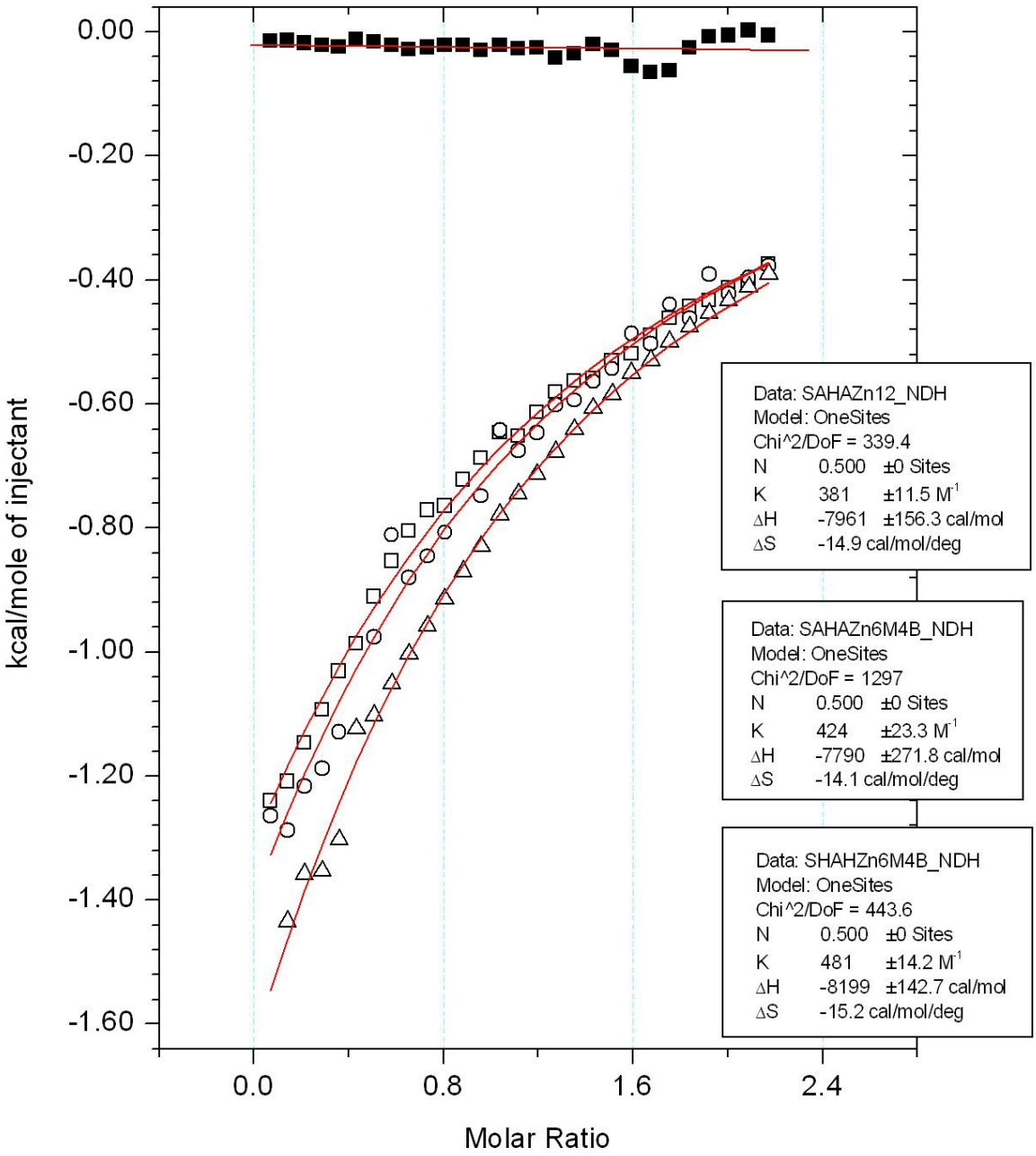

Figure 2.2: Fitting of SAHA into zinc(II) isotherms. *The three triplicate isotherms (open symbols) of 10 mM SAHA and 1 mM zinc(II) are shown with their corresponding best fit line. The methanol: buffer mixture into zinc(II) control (closed symbol) was subtracted from the binding isotherms before fitting the curve.*

The average binding parameters obtained when titrating SAHA into zinc(II) were an equilibrium constant of $4.3 \pm 0.5 \times 10^2\ M^{-1}$, a ΔH of $-8.0 \pm 0.2 \times 10^3$ cal/mol, a ΔS of -14.7 ± 0.6 cal/mol·deg, a $\Delta G°$ of -15.0 ± 0.3 kJ/mol and a stoichiometry of binding fixed at 0.5 SAHA per zinc ion, as shown in Table 2.1 and 2.2. The fitting was not able to find a unique n-value, a consequence of the c-value being outside of the ideal window. However, when the n-value was fixed at 0.5 or lower the fit was equally as good when judged by the naked eye. It is also important to note that the data did not fit n-values of 1 or greater, which was determined by comparing the values obtained for the reduced chi-squared. The stoichiometry of binding represents the number of moles of titrate bound per titrate, thus the stoichiometry of 0.5 implies that two zinc(II) ions are bound per SAHA molecule.

The rationale behind the n-value of 0.5 is somewhat unclear but several factors may be contributing to this unexpected value. The first is that the concentration of SAHA could have been underestimated or the concentration or zinc(II) could have been over estimated due to massing errors. Either scenario would result in a smaller n-value. The solution concentrations will be verified using atomic absorption spectroscopy (experiment not yet conducted). The more likely reasoning behind this unexpected value is that the solubility of SAHA is low. Because of this, the concentration of SAHA could not be increased enough to be in the ideal c-value window of 1-1000. Figure 2.2 shows that the curves are nearly featureless (refer to Figure 1.7 for the shape of an ideal curve), which explains why the curve fitting is unable to pinpoint an n-value. In addition, the value of the subtracted plateau heat alters the n-value. However, it is worth noting that the variance in stoichiometry of binding does not significantly affect the equilibrium binding constant (determined through fitting the same curve with multiple n-values and comparing the equilibrium constants obtained.)

The bond angle of the hydroxamic acid group on SAHA makes it extremely favorable to interact only with zinc(II), especially zinc(II) at the active site of HDAC.[40] The fairly large equilibrium constant of $4.3 \pm 0.5 \times 10^2\ M^{-1}$ suggests that the interaction of SAHA and zinc(II) is a strong interaction with little dissociation. Additionally, the ΔH value of $-8.0 \pm 0.2 \times 10^3$ cal/mol suggests a very exothermic reaction where heat is being released to the surroundings. The negative $\Delta G°$ is consistent with the reaction occurring spontaneously under standard state conditions. These data were unavailable prior to this study.

In addition to thermodynamic binding data, this study provides valuable insight into the major energetic contributors of HDAC inhibition. The equilibrium constant of $4.3 \pm 0.5 \times 10^2\ M^{-1}$ obtained in this study is small in comparison to the equilibrium constant for SAHA and zinc at the active site of HDAC8, $1.72 \times 10^6\ M^{-1}$.[16] This seems to suggest that the other interactions of SAHA such as the van der Waals interactions with the hydrophobic tunnel and the interactions of the cap on the surface of the enzyme are the major contributors to the affinity of SAHA for the active site. To compare in terms of the energetic binding, the $\Delta G°$, which has an additive relationship for contributions from different interactions rather than the multiplicative relationship of the affinity constant, was calculated from the K_a using Equation 6. The contribution of zinc binding seems to be more readily comprehended through the $\Delta G°$ for SAHA binding to zinc(II) of -15.0 kJ/mol as opposed to the $\Delta G°$ for SAHA interacting with the active site of HDAC8 of -35.6 kJ/mol.[16] These values suggest that the binding of SAHA to zinc(II) contributes approximately 42% of the binding energetics of the overall SAHA and zinc(II) interaction.

2.2 SAHA-Co^{2+} Binding in the Methanol: Buffer Mixture

The binding interaction of 20 mM SAHA and 3 mM cobalt(II) was also determined in the same methanol: buffer mixture described above. Figure 2.3 shows sample data obtained for a SAHA into cobalt(II) titration experiment. Figure 2.4 shows an overlay of five replicate binding isotherms obtained under the same experimental conditions. The cobalt(II) controls and plateau heats were subtracted from each binding isotherm as described above.

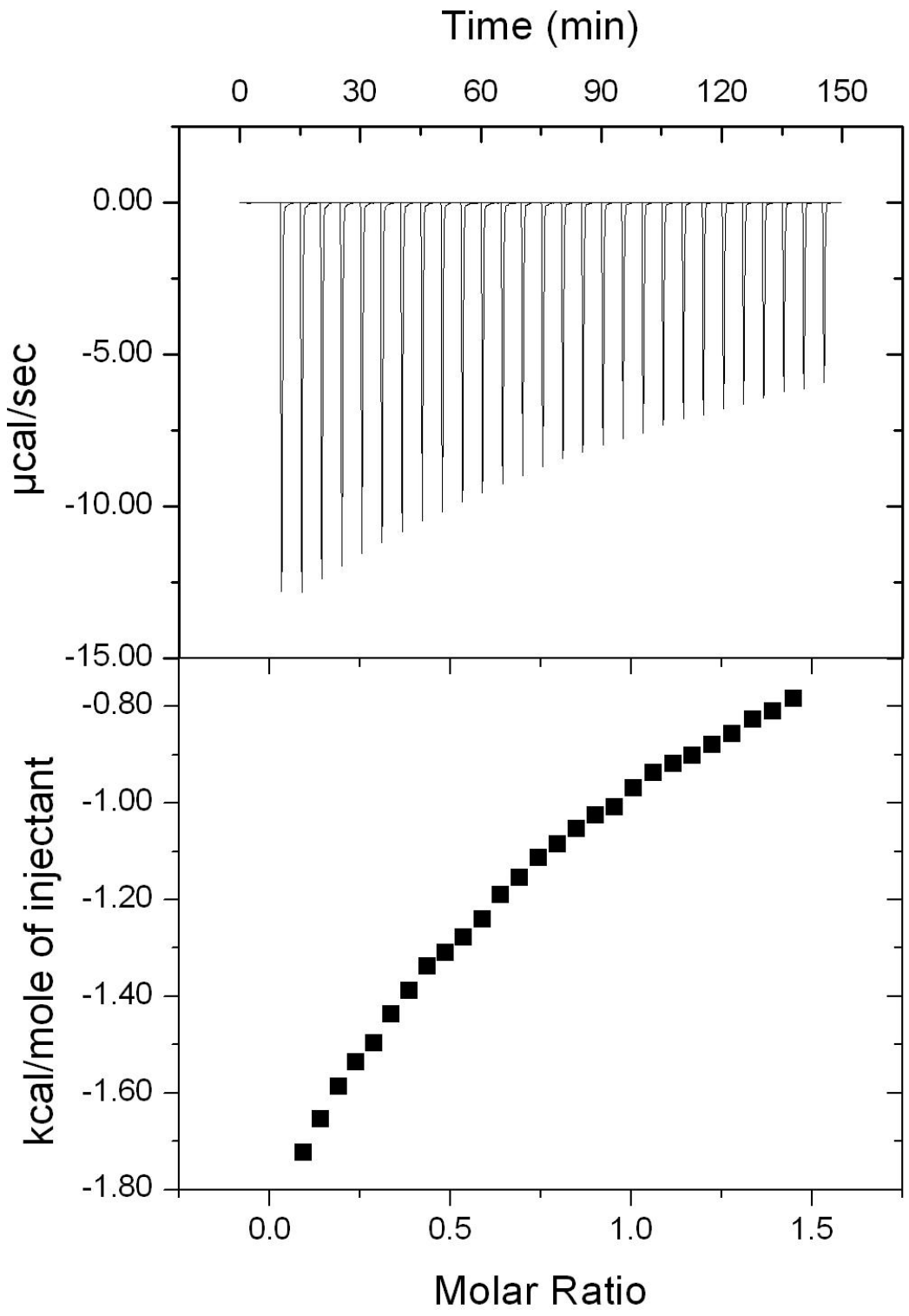

Figure 2.3: Titration calorimetry of SAHA into cobalt(II). *A 10 mM solution of SAHA and a 3 mM solution of cobalt (II) were prepared in 60% anhydrous methanol and 40% 50 mM NEM, 150 mM NaCl buffer pH 6.80. SAHA was titrated into cobalt(II) at 25°C using 10 µL injections.*

The average binding parameters obtained for titrating SAHA into cobalt(II) were a stoichiometry of binding fixed at 0.50 SAHA per cobalt(II), an equilibrium binding constant of $2.0 \pm 0.5 \times 10^2\ M^{-1}$, a ΔH of $-5.6 \pm 0.7 \times 10^3$ cal/mol, a ΔS of -8.5 ± 2.7 cal/mol·deg and a $\Delta G°$ of -13.1 ± 0.7 kJ/mol (Table 2.1 and 2.2). The stoichiometry of binding implies that two cobalt(II) ions are bound per SAHA molecule. This, like the SAHA-zinc(II) curves, is most likely due to the small c-value of approximately 0.3 causing the undesirable shape of the binding curves. This required the n-value to be fixed at 0.5 because when the curve was fit the program could not settle on a unique set of parameters.

Using cobalt(II) as a point of comparison, the fairly small equilibrium constant of $2.0 \pm 0.5 \times 10^2\ M^{-1}$ suggests that the interaction of SAHA with cobalt(II) is approximately half the strength of the interaction between SAHA and zinc(II), which has an equilibrium constant of $4.3 \pm 0.5 \times 10^2\ M^{-1}$. While the stoichiometric ratio of SAHA and cobalt(II) and SAHA and zinc(II) are the same (1:2) the difference in equilibrium constants suggests that SAHA is bound more tightly to zinc(II) than it is to cobalt(II). These values imply that when using the same concentrations of zinc(II) and cobalt(II) fewer SAHA molecules dissociated from zinc(II) than dissociated from cobalt(II). Additionally, the 110° bond angle of the hydroxamic acid favors zinc(II) due to its ideal orientation around zinc(II) to form a penta-coordinated ion.[41] This seems to be a plausible reason as to why zinc(II) binds more strongly to SAHA than cobalt(II). Again, the calculated $\Delta G°$ of -13.1 ± 0.7 kJ/mol compared to the $\Delta G°$ of -15.0 ± 0.3 kJ/mol for SAHA and zinc(II) binding shows that cobalt(II) binding energetically contributes approximately 13% less than zinc(II) binding.

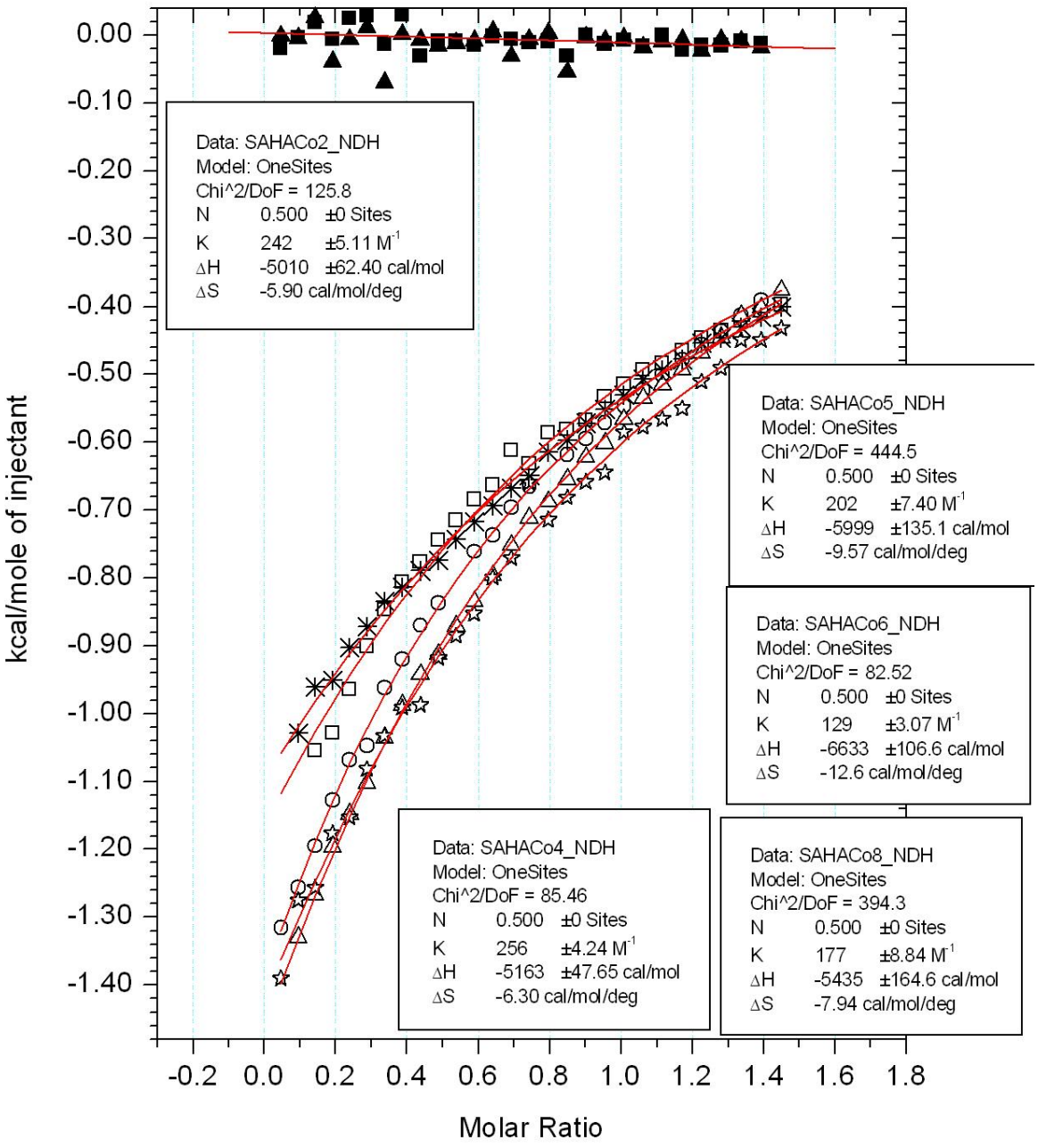

Figure 2.4: Fitting of SAHA into cobalt(II) isotherms. *An overlay of the binding isotherms from three triplicate experiments of 20 mM SAHA into 3 mM cobalt(II) are shown (open symbols). The cobalt(II) controls (closed symbols) were averaged and then subtracted from the binding curves.*

2.3 AHA-Zn^{2+} Binding in the Methanol: Buffer Mixture

To relate the binding parameters obtained for SAHA in the methanol: buffer mixture to more physiological conditions, we chose to also study the water, as well as methanol soluble compound AHA (Figure 2.5). Acetohydroxamic acid shares the chemical structure with the portion of SAHA (Figure 1.6) responsible for coordinating to zinc ions, the hydroxamic acid, in the active site of HDACs and is used in the literature as the prototype for hydroxamic acid binding. Acetohydroxamic acid interacting with zinc(II) and cobalt(II) was studied in both the solvent mixture and aqueous buffer. The difference between the data for AHA-metal binding in the solvent mixture compared to aqueous conditions was used to extrapolate SAHA-metal binding in buffer.

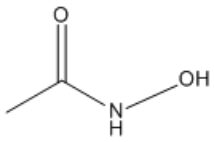

AHA

Figure 2.5: Skeletal structure of acetohydroxamic acid.

The binding interaction of 20 mM AHA into 2 mM zinc(II) was determined in the methanol: buffer mixture. Figure 2.6 shows raw data and the resulting binding isotherm for a sample AHA into zinc(II) titration experiment. Figure 2.7 shows an overlay of the isotherms of five replicate experiments. On the same figure are two AHA controls, which were averaged and then subtracted from each of the binding curves. A plateau value was subtracted as described for previous titration experiments

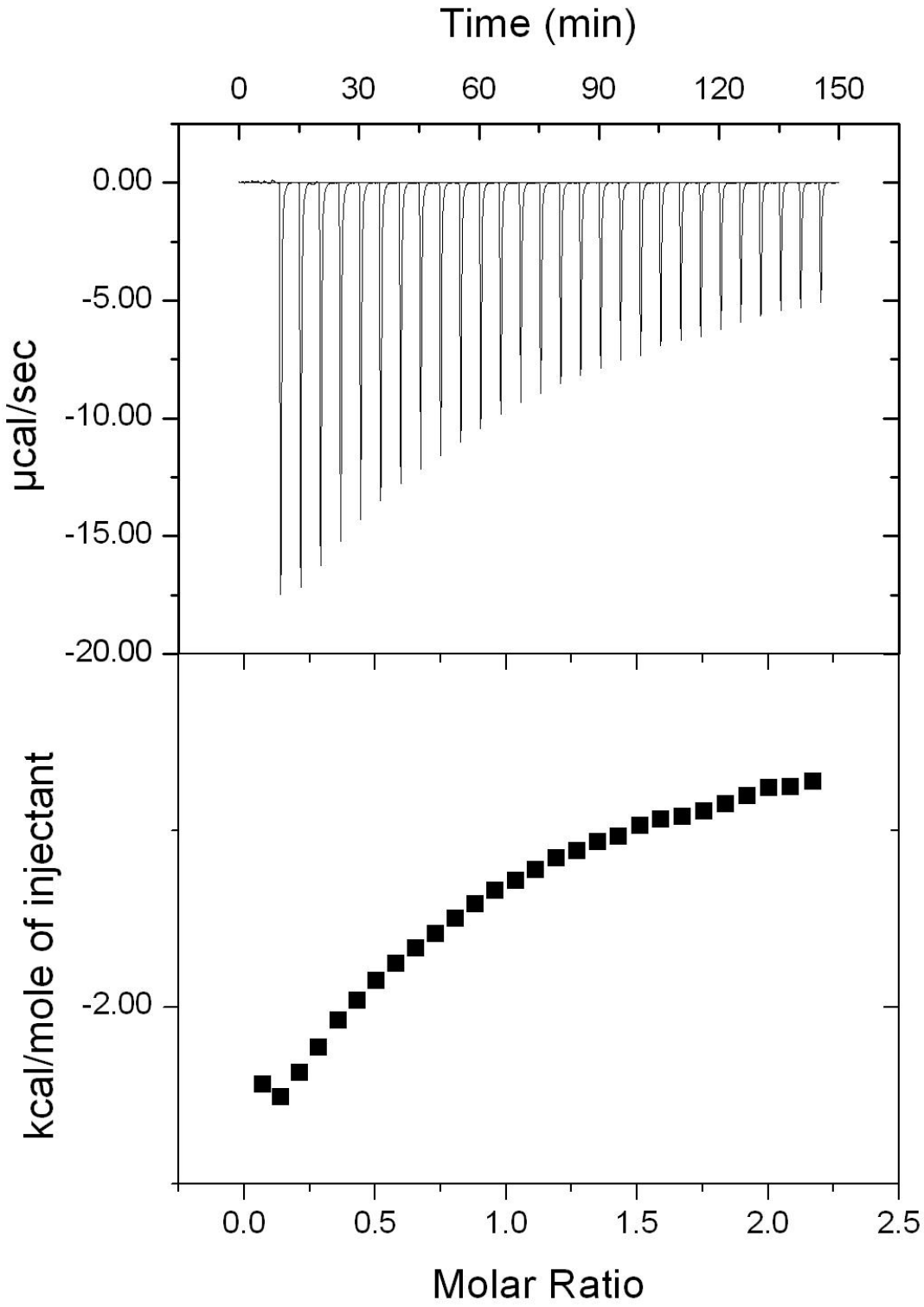

Figure 2.6: Titration calorimetry of AHA into zinc(II). *A 20 mM solution of AHA and a 2 mM solution of zinc(II) were prepared in 60% anhydrous methanol and 40% 50 mM NEM, 150 mM NaCl buffer pH 6.80. The AHA solutions were titrated at 25°C into zinc(II) using 10 µL injections.*

The average binding parameters obtained for 20 mM AHA and 2 mM zinc(II) are an n-value of 0.52 ± 0.17 AHA per zinc(II), an equilibrium constant of 4.4 ± 0.8 $x10^2$ M^{-1}, a ΔH of -8.6 ± 3.2 $x10^3$ cal/mol, a ΔS of -17 ± 11 cal/mol·deg and a ΔG° of -15.0 ± 0.5 kJ/mol (Table 2.1 and 2.2). Acetohydroxamic acid is not a known HDAC inhibitor, thus the relevance of these data is not to determine the binding strength of AHA and zinc(II) compared to that of SAHA and zinc(II). Rather, these data will be compared to the data obtained for AHA and zinc(II) in buffer to establish if the parameters drastically change under the two different solvent conditions.

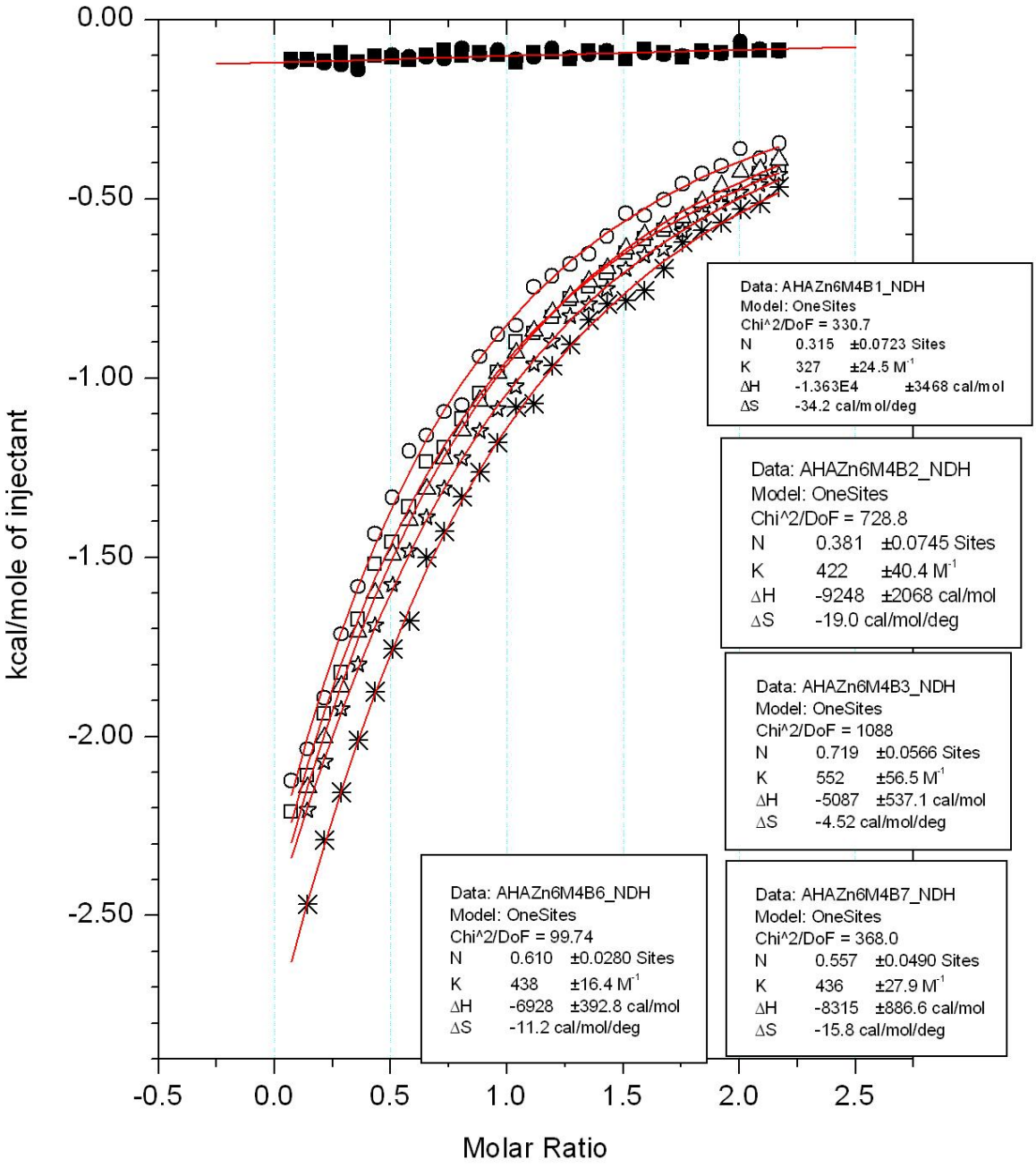

Figure 2.7: Fitting of AHA into zinc(II) isotherms. *An overlay of the five replicate titrations of AHA into zinc(II) at the given concentration is shown with the open symbols. The AHA controls are shown with the closed symbols. The controls were averaged and then subtracted from each binding curve before fitting the curve.*

2.4 AHA-Co^{2+} Binding in the Methanol: Buffer Mixture

The binding interaction of 20 mM AHA and 2 mM cobalt(II) was determined in the methanol:buffer mixture. Figure 2.8 shows raw data and the resulting binding isotherm for a sample AHA into cobalt(II) titration experiment. Figure 2.9 shows an overlay of the isotherms of five replicate experiments. The AHA controls as well as a plateau heat were subtracted as previously described.

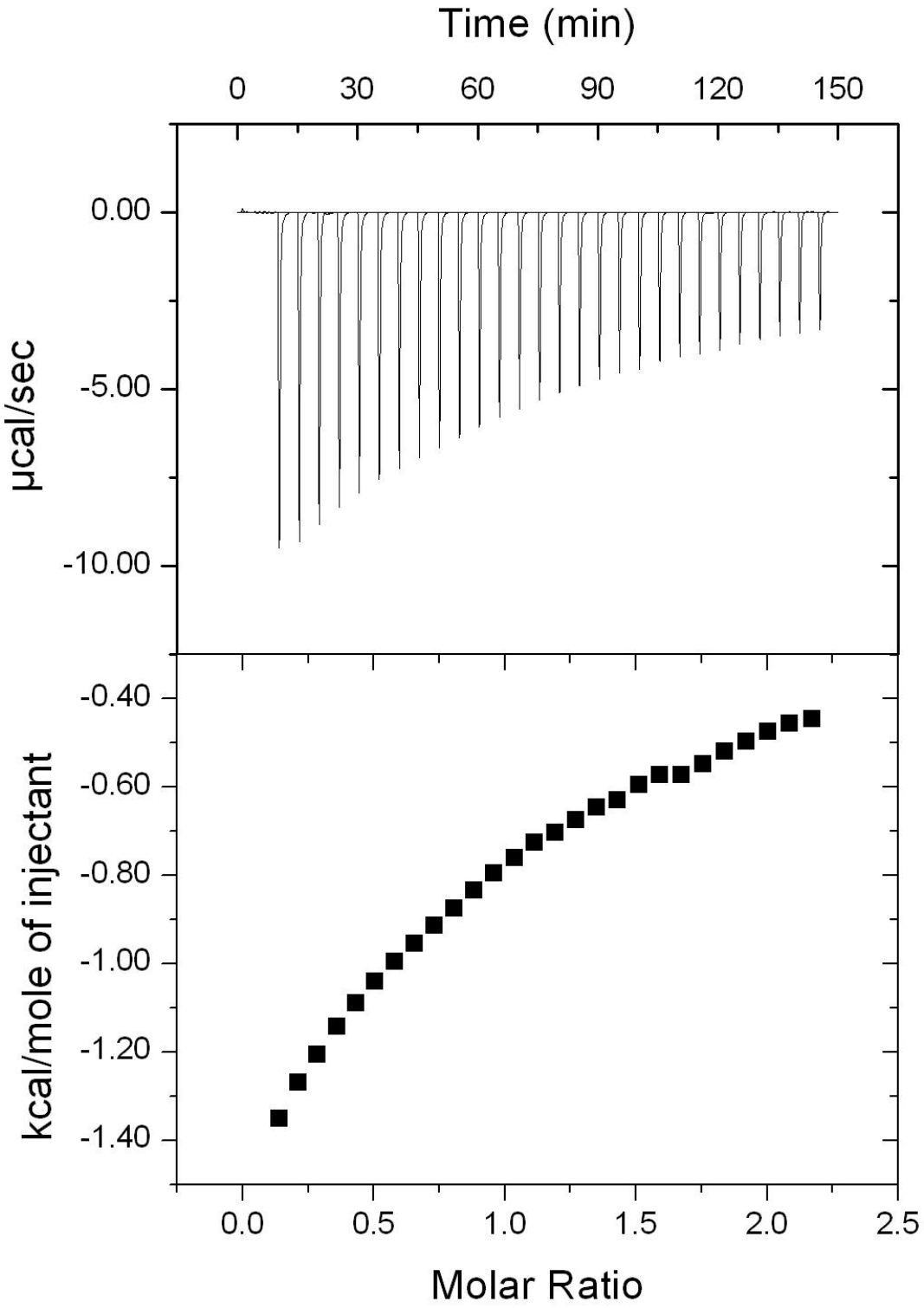

Figure 2.8: Titration calorimetry of AHA into cobalt(II). *A 20 mM solution of AHA and a 2 mM solution of cobalt(II) were prepared in 60% anhydrous methanol and 40% 50 mM NEM, 150 mM NaCl buffer pH 6.80. The AHA solutions were titrated into cobalt(II) at 25°C using 10 µL injections.*

The average binding parameters obtained for 20 mM AHA and 2 mM cobalt(II) are an n-value of 0.58 ± 0.12 AHA per cobalt(II), an equilibrium binding constant of $3.2 \pm 0.4 \times 10^2\ M^{-1}$, a ΔH of $-5.0 \pm 1.2 \times 10^3$ cal/mol, a ΔS of -5 ± 4 cal/mol·deg and a $\Delta G°$ of -14.3 ± 0.4 kJ/mol (Table 2.1 and 2.2). Like the data obtained for the interaction of AHA and zinc(II), these data were not used for determining binding strength of AHA and cobalt(II) compared to that of SAHA and cobalt(II) but rather to compare the interaction of AHA and the metal across the two solvent conditions.

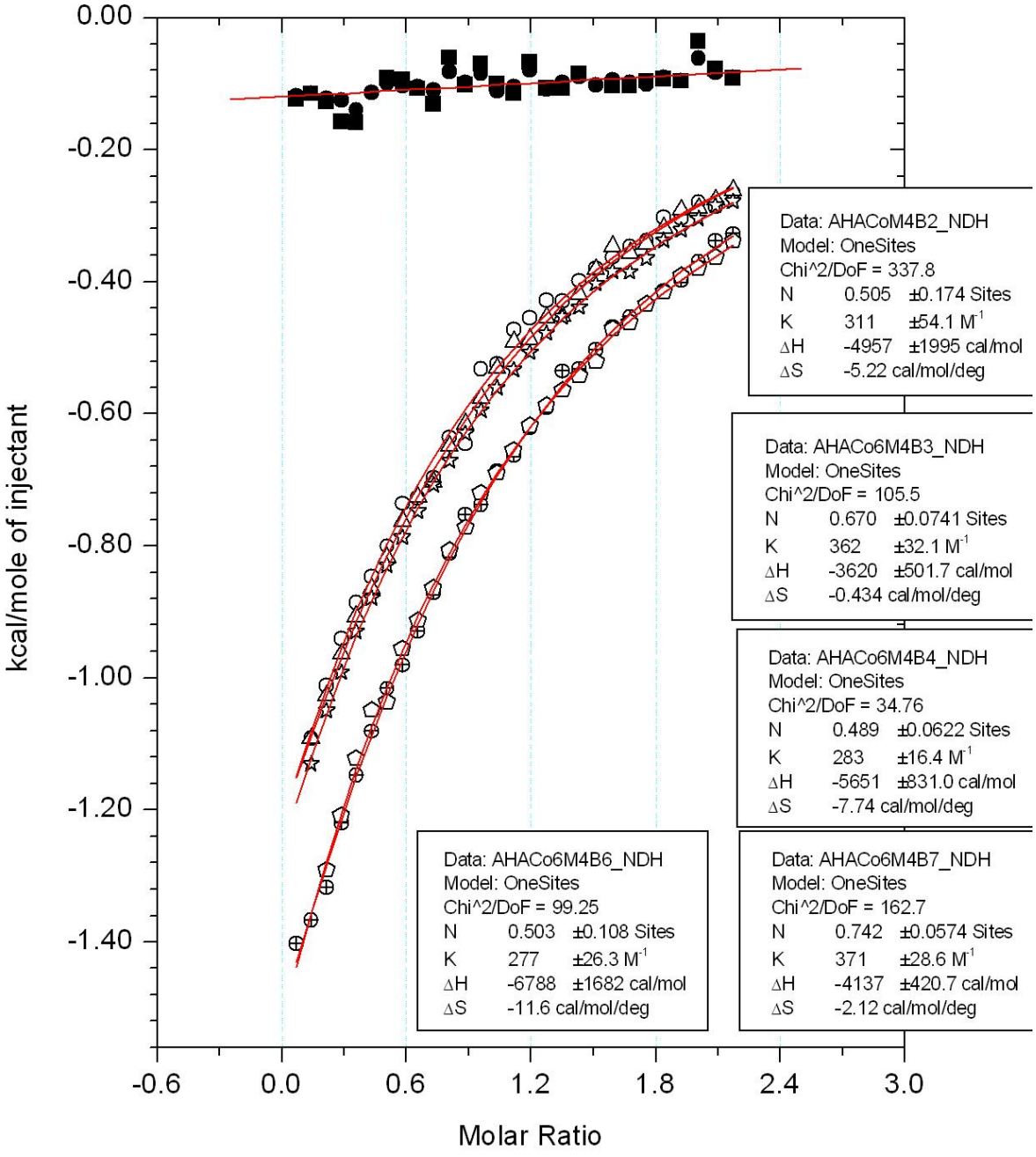

Figure 2.9: Fitting of AHA into cobalt(II) isotherms. *An overlay of the five replicate titration experiments of 20 mM AHA into 2 mM cobalt(II) is shown (open symbols). The AHA controls are shown with the solid symbols. The controls were averaged and then subtracted from each binding curve before fitting the each isotherm.*

2.5 AHA-Zn^{2+} Binding in Buffer

To determine the differences in the thermodynamic binding parameters between the methanol: buffer mixture and aqueous conditions, the interaction of 50 mM AHA and 5 mM zinc(II) was determined in NEM buffer. Figure 2.10 shows raw data and the resulting binding isotherm for a sample AHA into zinc(II) titration experiment. Figure 2.11 shows an overlay of the isotherms of four replicate experiments. The AHA controls and plateau heat was subtracted as described for previous titration experiments.

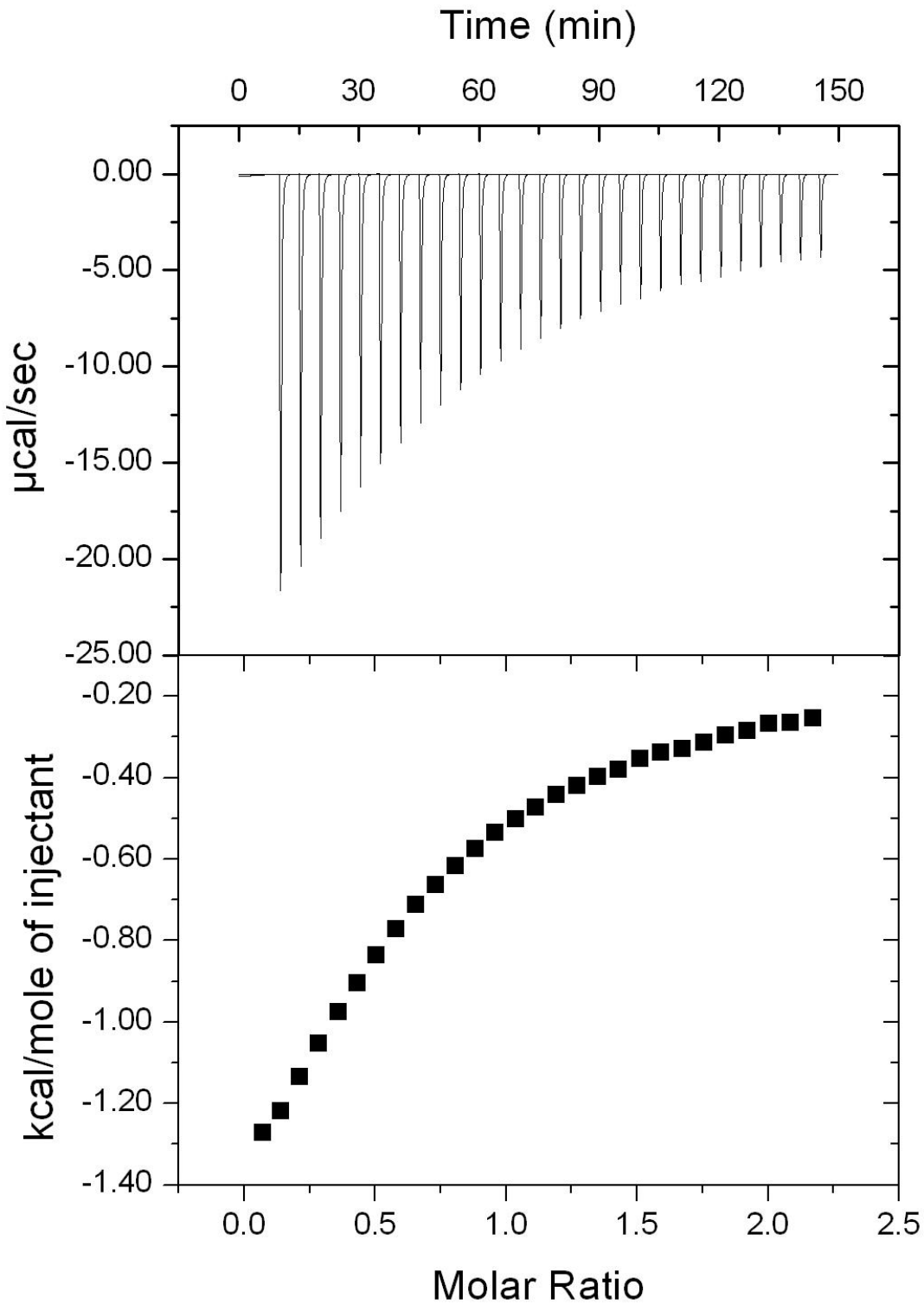

Figure 2.10: Titration calorimetry of AHA into zinc(II). *A 50 mM solution of AHA and a 5 mM solution of zinc(II) were prepared in 50 mM NEM, 150 mM NaCl buffer pH 6.80. The AHA solutions were titrated into zinc(II) at 25°C using 10 µL injections.*

The average binding parameters obtained for 50 mM AHA and 5 mM zinc(II) are an n-value of 0.51 ± 0.06 AHA per zinc(II), an equilibrium constant of 3.6 ± 0.4 x10^2 M^{-1}, a ΔH of -2.5 ± 0.2 x10^3 cal/mol, a ΔS of 3.2 ± 0.3 cal/mol·deg and a ΔG° of -14.6 ± 0.8 kJ/mol (Table 2.1 and 2.3). When comparing the stoichiometry and equilibrium binding constants obtained in buffer to those obtained in the methanol: buffer mixture the n-value of 0.51 ± 0.06 AHA per zinc(II) obtained in buffer and 0.52 ± 0.17 AHA per zinc(II) obtained in the methanol: buffer mixture agree. The equlibrium binding constants are also the same within error between the methanol: buffer mixture and buffer; 4.4 ± 0.8 x 10^2 and 3.6 ± 0.4 x 10^2 M^{-1}, respectively.

However, the ΔH and ΔS are vastly different between the two solvent conditions. These significant differences (ΔH_{buffer}= -2.5 ± 0.3 x10^3 cal/mol, ΔS_{buffer}= 3.15 ± 0.75 x10^3 cal/mol·deg, $\Delta H_{mixture}$= -8.6 ± 3.2 x10^3 cal/mol, and $\Delta S_{mixture}$= -17 ±11 cal/mol·deg) can be attributed to both ΔH and ΔS depending on solvation and desolvation. The solvation and desolvation process differs from one solvent to another; in this case, the solvation enthalpy under aqueous conditions would be greater than in the methanol:buffer mixture for the polar moiety. Thus we would expect the equiblibrium constant to be larger in the mixture of solvents than in buffer. This is because the titrant and titrate have to forfeit less enthalpy to undergo desolvation to interact with each other. In addition, the idea of entropy-enthalpy compensation is observed in this system. This implies that although the values of entropy and enthalpy change between the two solvent conditions the relative difference between them is the same (i.e. a large negative enthalpy is accompained by a more negative entropy change and vice versa).

Overall, we can say that stoichiometry, binding affinity and ΔG° observed for AHA interacting with zinc(II) in the methanol: buffer mixture compared to those observed in buffer are the same. Because of this, the parameters for SAHA interacting with zinc(II) can be extrapolated

to buffer conditions. Based on the data obtained for the AHA zinc(II) interaction it is likely that the parameters acquired for the SAHA-zinc(II) interaction are very similar to what they would be if SAHA were soluble in aqueous condtions.

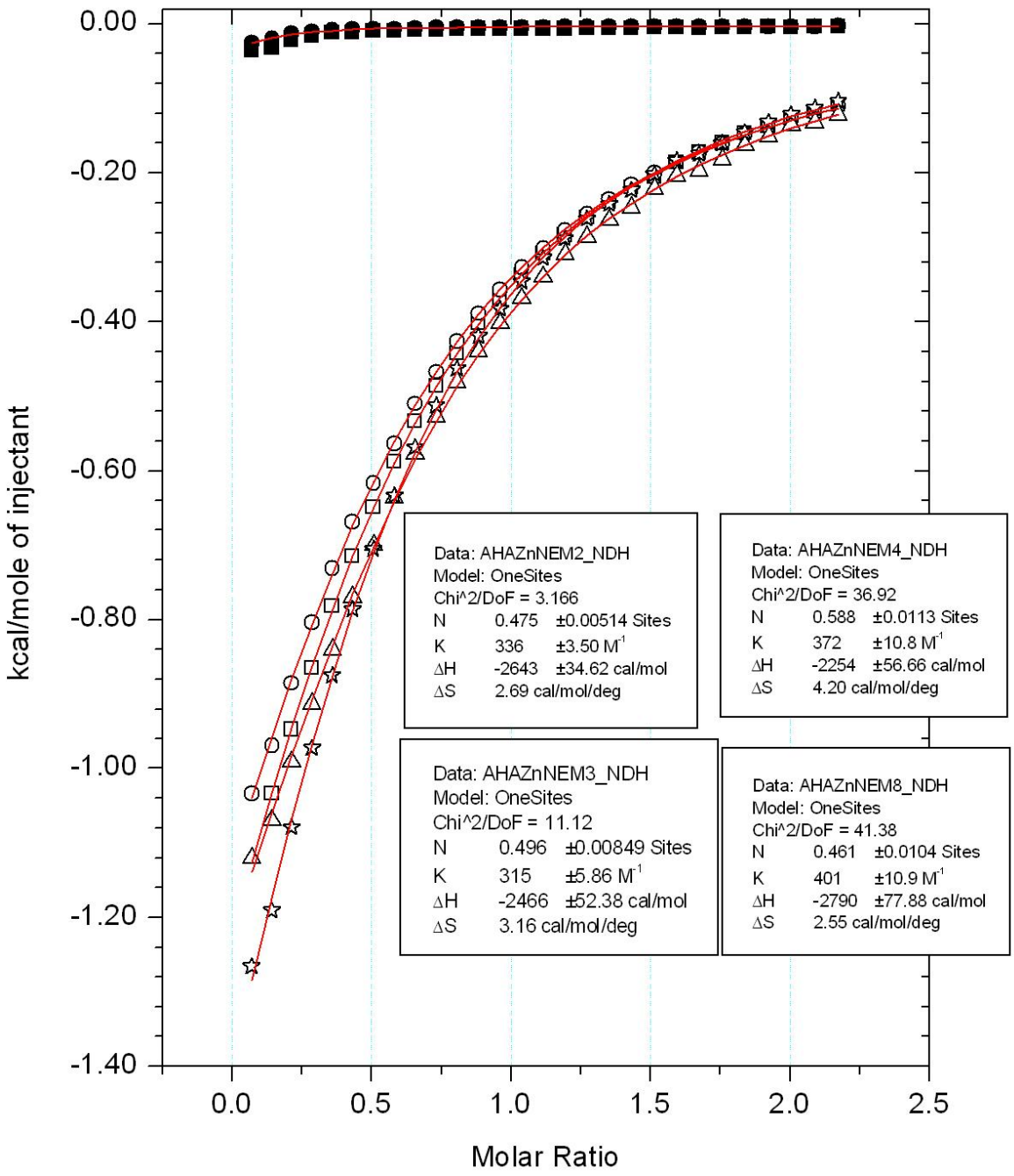

Figure 2.11: Fitting of AHA into zinc(II) isotherms. *An overlay of the four replicate experiments of 50 mM AHA into 5 mM zinc(II) is shown with the open symbols. The AHA controls are shown with the solid symbols. The controls were averaged and then subtracted from each binding curve before fitting the curve.*

In order to increase the c-value to better define the shape of the curve the concentrations of AHA and zinc(II) were doubled. This allowed for a more accurate determination of the binding parameters, especially the n-value. The experiments using the increased concentration were only able to be completed for AHA because SAHA has limited solubility under the chosen solvent conditions. Therefore, the binding interaction of 100 mM AHA and 10 mM zinc(II) was determined in buffer. Figure 2.12 shows raw data and the resulting binding isotherm for a sample AHA into zinc(II) titration experiment at the higher concentration. Figure 2.13 shows an overlay of the isotherms of two duplicate experiments. As described with previous titration experiments, the AHA controls and plateau heat was subtracted.

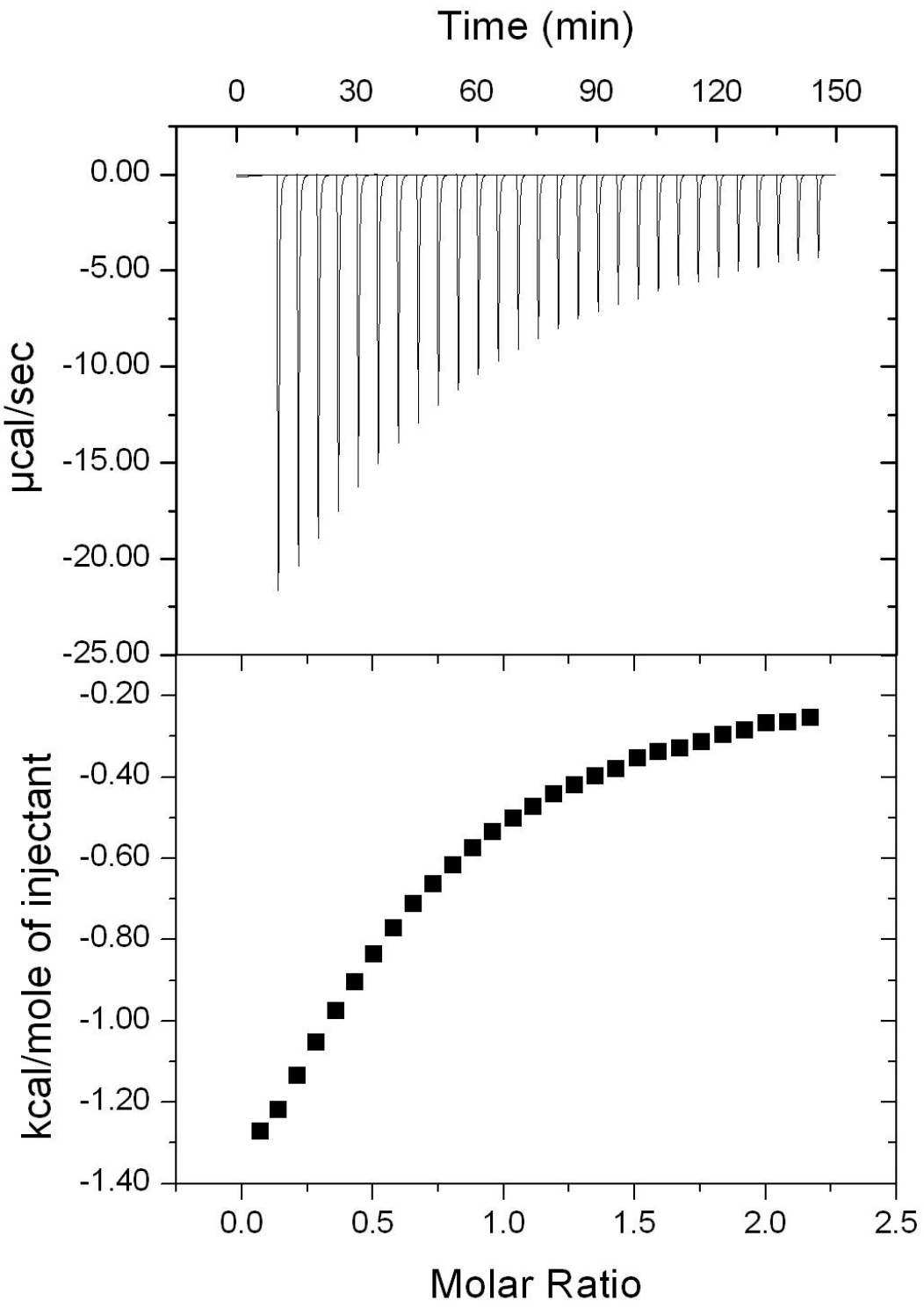

Figure 2.12: Titration calorimetry of AHA into zinc(II). *A 100 mM solution of AHA and a 10 mM solution of zinc(II) were prepared in 50 mM NEM, 150 mM NaCl buffer pH 6.80. The AHA solutions were titrated into zinc(II) at 25°C using 5 µL injections.*

The average binding parameters obtained for 100 mM AHA and 10 mM zinc(II) are an n-value of 0.33 ± 0.06 AHA per zinc(II), an equilibrium binding constant of 6.5 ± 0.2 $x10^2$ M^{-1}, a ΔH of -2.5 ± 0.2 $x10^2$ cal/mol, a ΔS of 4.57 ± 0.69 cal/mol·deg and a $\Delta G°$ of -16.1 ± 0.1 kJ/mol (Tables 2.1 and 2.3). When comparing the data obtained using 100 mM AHA and 10 mM zinc(II) to the data obtained using 50 mM AHA and 5 mM zinc(II) it seems that the n-value is signficantly less, even with the associated error; 0.51 ± 0.06 sites obtained using 50 mM AHA and 5 mM zinc(II) compared to 0.33 ±0.06 sites obtained using 100 mM AHA and 10 mM zinc(II). The equilibrium binding constant is approximately doubled when the concentration of titrant and titrate are doubled, 3.4 ± 0.4 x 10^2 M^{-1} using 50 mM and 5 mM compared to 6.5 ± 0.2 x 10^2 M^{-1} obtained using 100 mM and 10 mM. These differences using the two concentrations suggests that the parameters obtained using the higher concentrations are more accurate because the c-value is within the ideal range of 1-1000 (3.26 compared to 0.84 with the lower concentrations).

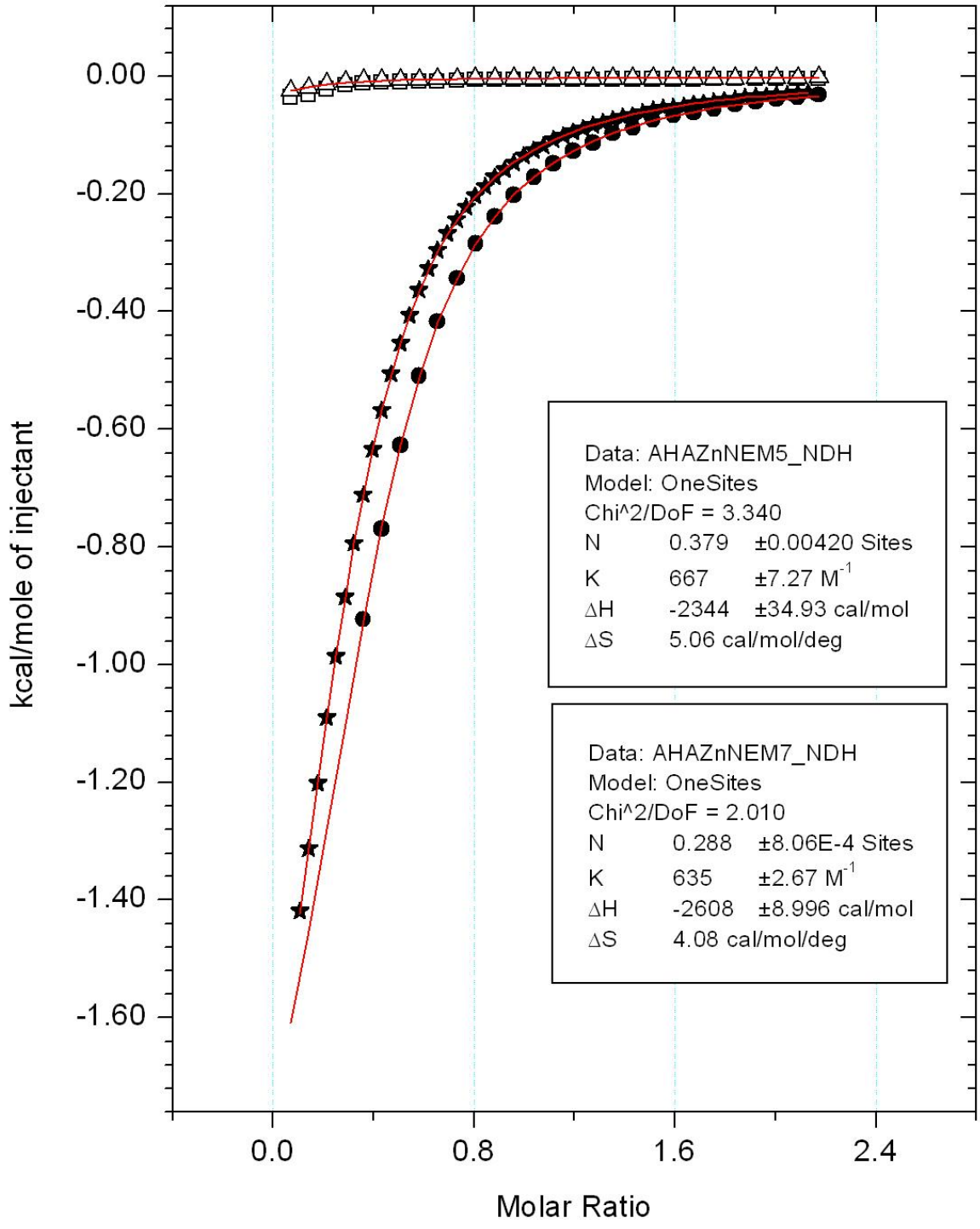

Figure 2.13: Fitting of AHA into zinc(II) isotherms. *Overlays of the two duplicate titration experiments of 100 mM AHA into 10 mM zinc(II) are shown with closed symbols. The AHA controls are shown with open symbols. The controls were averaged and then subtracted from each isotherm before fitting the binding curve.*

2.6 AHA-Co^{2+} Binding in Buffer

The binding interaction of 50 mM AHA and 5 mM cobalt(II) was determined in NEM buffer. Figure 2.14 shows raw data and the resulting binding isotherm for a sample AHA into cobalt(II) titration experiment. Figure 2.15 shows an overlay of the isotherms of three triplicate experiments. The AHA controls and plateau heat was subtracted as described for previous titration experiments.

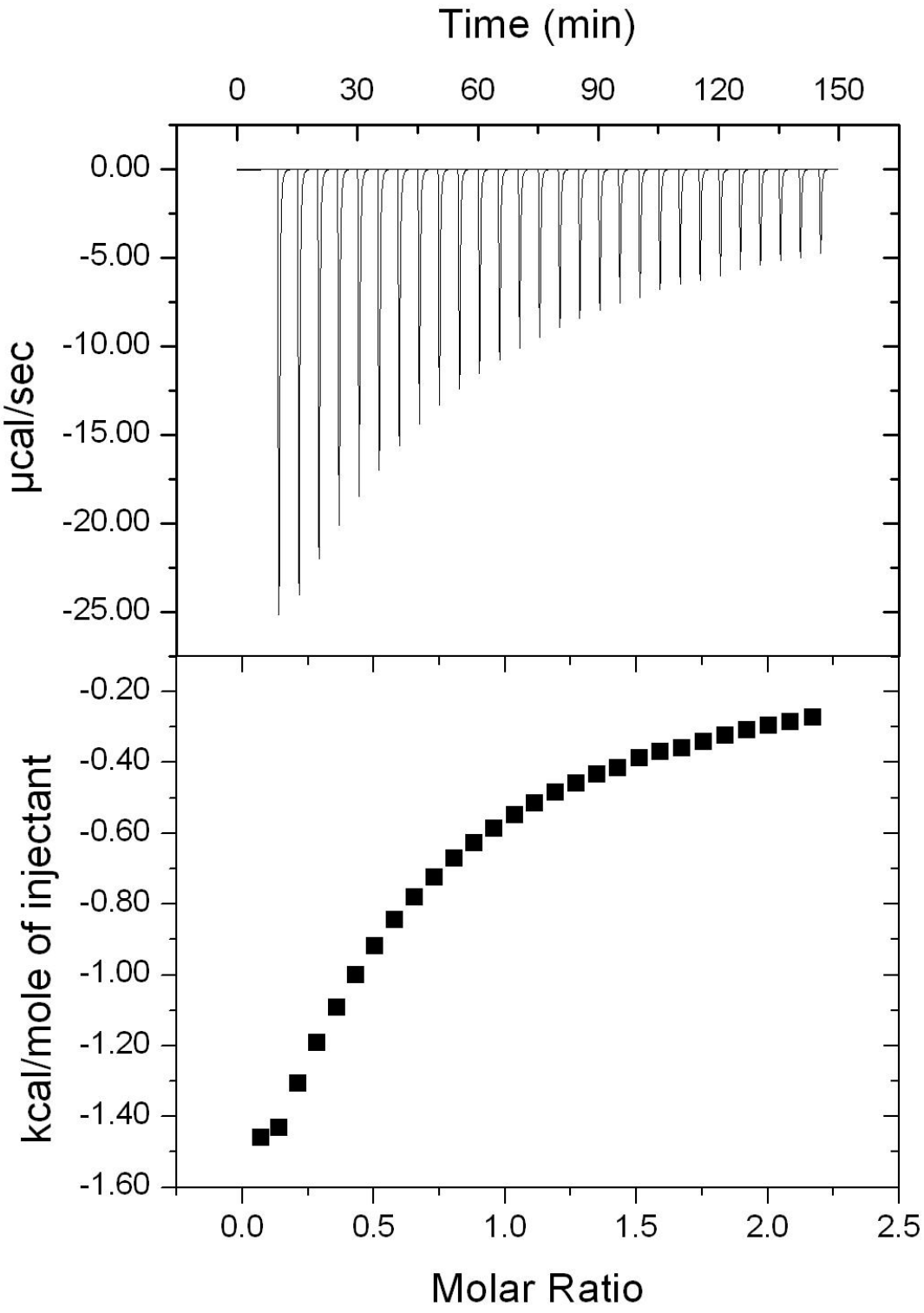

Figure 2.14: Titration calorimetry of AHA into cobalt(II)*. A 50 mM solution of AHA and a 5 mM solution of cobalt(II) were prepared in 50 mM NEM, 150 mM NaCl buffer, pH 6.80. The AHA solutions were titrated into cobalt(II) at 25°C using 10 µL injections.*

The average binding parameters obtained for 50 mM AHA and 5 mM cobalt(II) are an n-value of 0.26 ± 0.01 AHA per cobalt(II), an equilibrium constant of 2.1 ± 0.3 x10^2 M^{-1}, a ΔH of -7.2 ± 0.3 x10^3 cal/mol, a ΔS of -13.5 ± 1.0 cal/mol·deg and a ΔG° of -13.2 ± 0.1 kJ/mol (Tables 2.1 and 2.3). The data obtained in buffer compared to the data obtained in the methanol: buffer mixture suggest that the values obtained between the two solvent condtions are not the same within error. However, a fitting with the n-value fixed at 0.5 also fits the data, although based on the reduced chi-squared, not as well as the curve that yielded the values stated previously. This implies that the curve is not unique enough to fit just one set of parameters due to the low c-value of 0.27. Additionally, the equiblibrium binding constants of 3.0 ± 0.4 x10^2 M^{-1} agree within error of the 3.2 ± 0.5 x10^2 M^{-1} determined in the methanol:buffer mixture. Therefore, we concluded that the parameters obtained in the methanol:buffer mixture and in NEM buffer are comparable. Additionally, the thermodynamic binding parameters for the interaction of SAHA and cobalt(II) in buffer can be extrapolated, although these values are most likely not as accurate as those obtained from the interaction of SAHA and zinc(II). This is because the AHA-Co(II) parameters were not as agreeable between the two solvents as those obtained for AHA and zinc. Again, the entropy and enthalpy were not used as part of the comparision because they change with relation to other factors unrelated to the heat of binding.

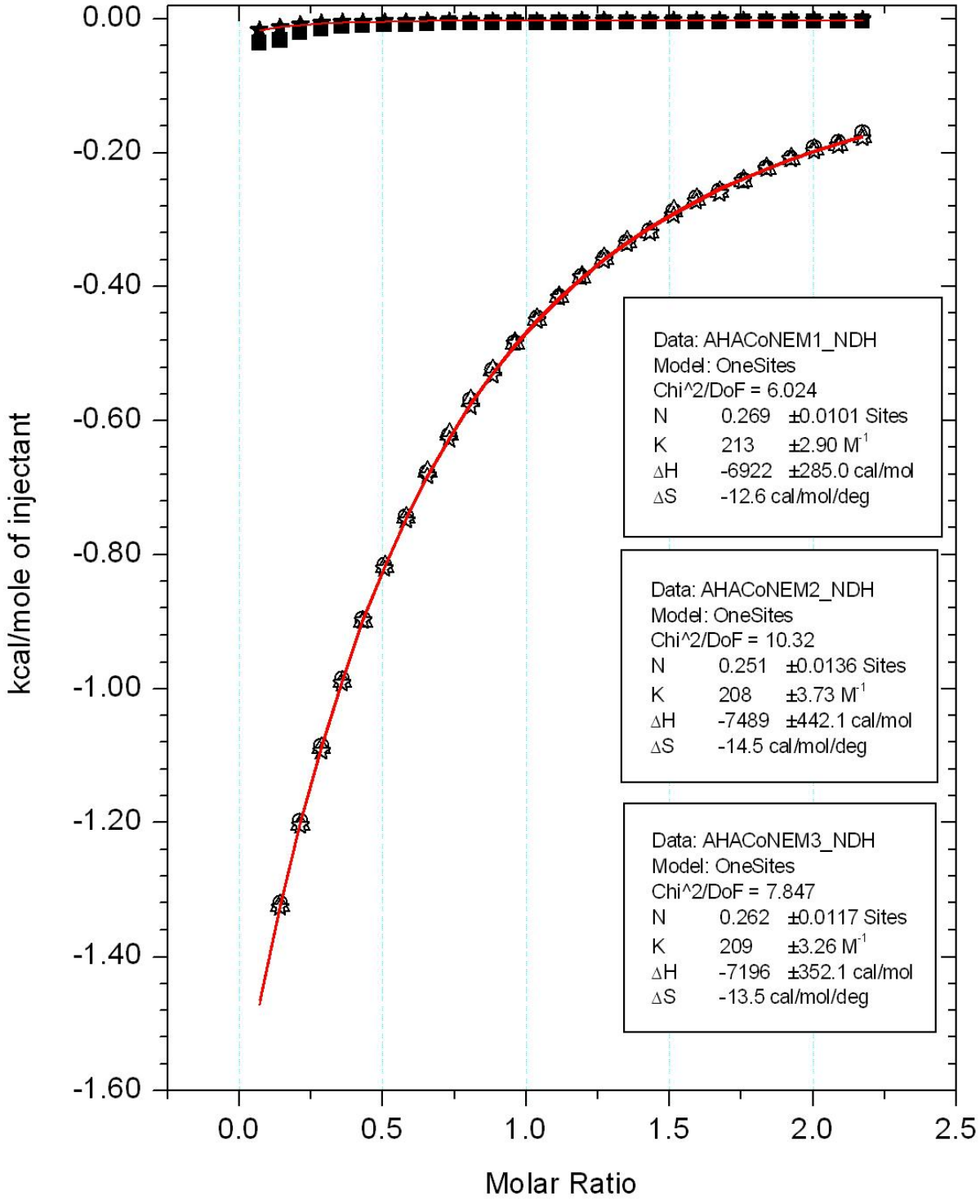

Figure 2.15: Fitting of AHA into cobalt(II) isotherms. *An overlay of the three duplicate titration experiments of 50 mM AHA into 5 mM cobalt(II) is shown with the open symbols. The AHA controls are shown with the closed symbols. The controls were averaged and then subtracted from each isotherm before fitting the curve. Another run was performed using the same conditions but was not shown on the curve because it looked identical to the previous runs.*

To confirm the binding parameters and determine whether or not the different injection order (i.e. higher local concentration of AHA rather than cobalt(II)) results in a different binding mode, cobalt(II) was titrated into AHA, the opposite of the previous runs. Thus the binding interaction of 50 mM cobalt(II) into 5 mM AHA was determined in buffer. Figure 2.16 shows raw data and the resulting binding isotherm for a sample cobalt(II) into AHA titration experiment. Figure 2.17 shows an overlay of the isotherms of three triplicate experiments. The cobalt control and plateau heat were subtracted as previously described. It is important to note that this type of experiment could not be conducted using zinc because of its limited solubility under the chosen solvent conditions.

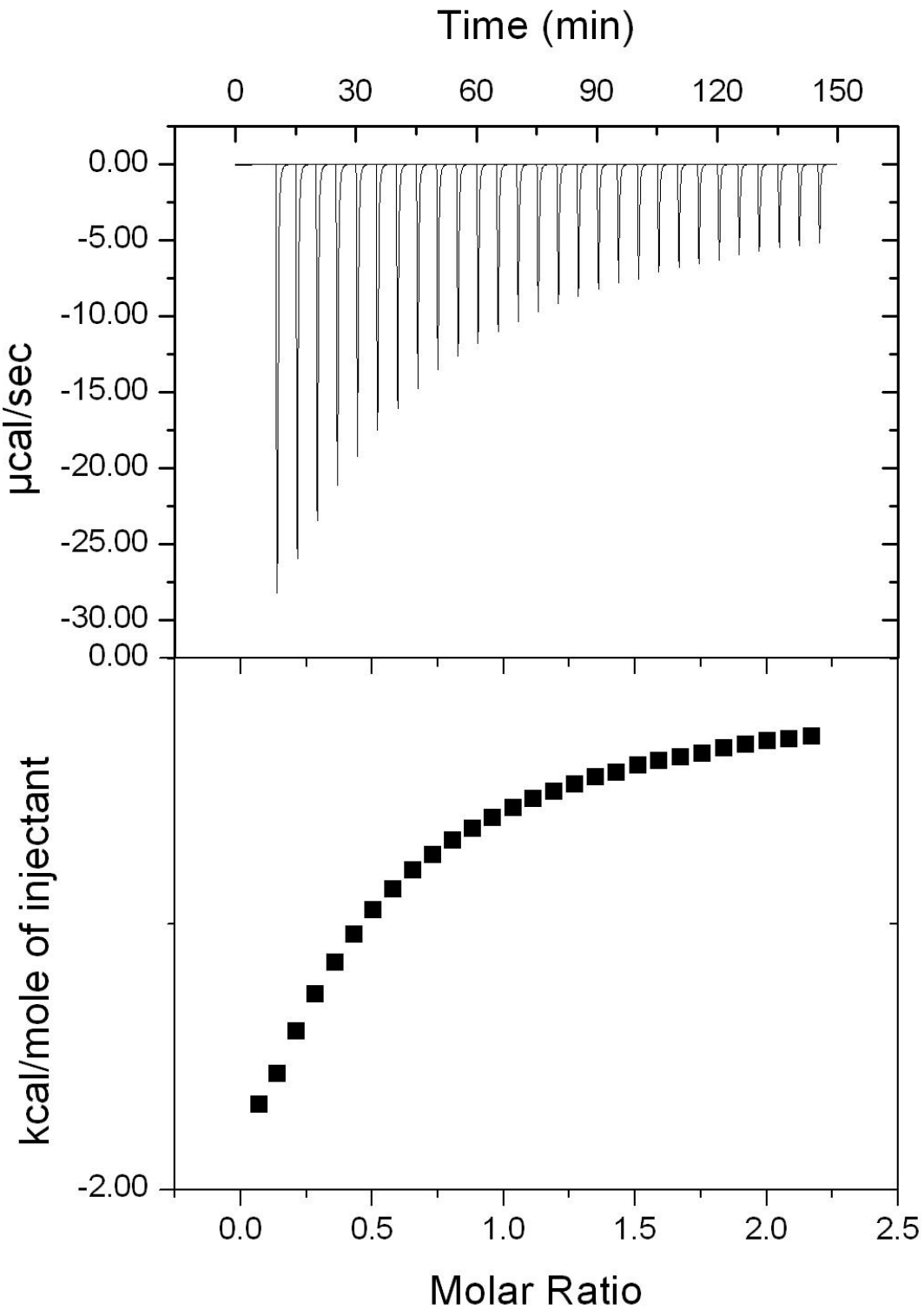

Figure 2.16: Titration calorimetry of Cobalt(II) into AHA. *A 50 mM solution of $CoCl_2$ and a 5 mM solution of AHA were prepared in 50 mM NEM, 150 mM NaCl buffer pH 6.80. The cobalt(II) solutions were titrated into AHA at 25°C using 10 µL injections.*

The average binding parameters obtained when titrating 50 mM cobalt(II) and 5 mM AHA are an n-value of 0.23 ± 0.08 cobalt(II) per AHA, an equilibrium binding constant of 2.8 ± 0.6 x10^2 M^{-1}, a ΔH of -7.8 ± 2.2 x10^3 cal/mol, a ΔS of -15.1 ± 7.9 cal/mol·deg and a ΔG° of -13.9 ± 0.5 kJ/mol (Tables 2.1 and 2.3). When comparing these data to the data obtained when titrating AHA into cobalt(II), the values for K_a are within error of each other. However, the stoichiometry of binding, is changed significantly when the local concentration of AHA and cobalt(II) are changed. This could be caused by an actual shift in the binding mode or simply just error with the experiment or an error in the data analysis caused by the low c-value due to solubility constraints. Despite the differences in the n-value, the affinity is the same and is not dependent on the local concentration of one molecule over the other. This suggests that the equilibrium binding constant obtained for AHA and cobalt(II) in buffer is reliable.

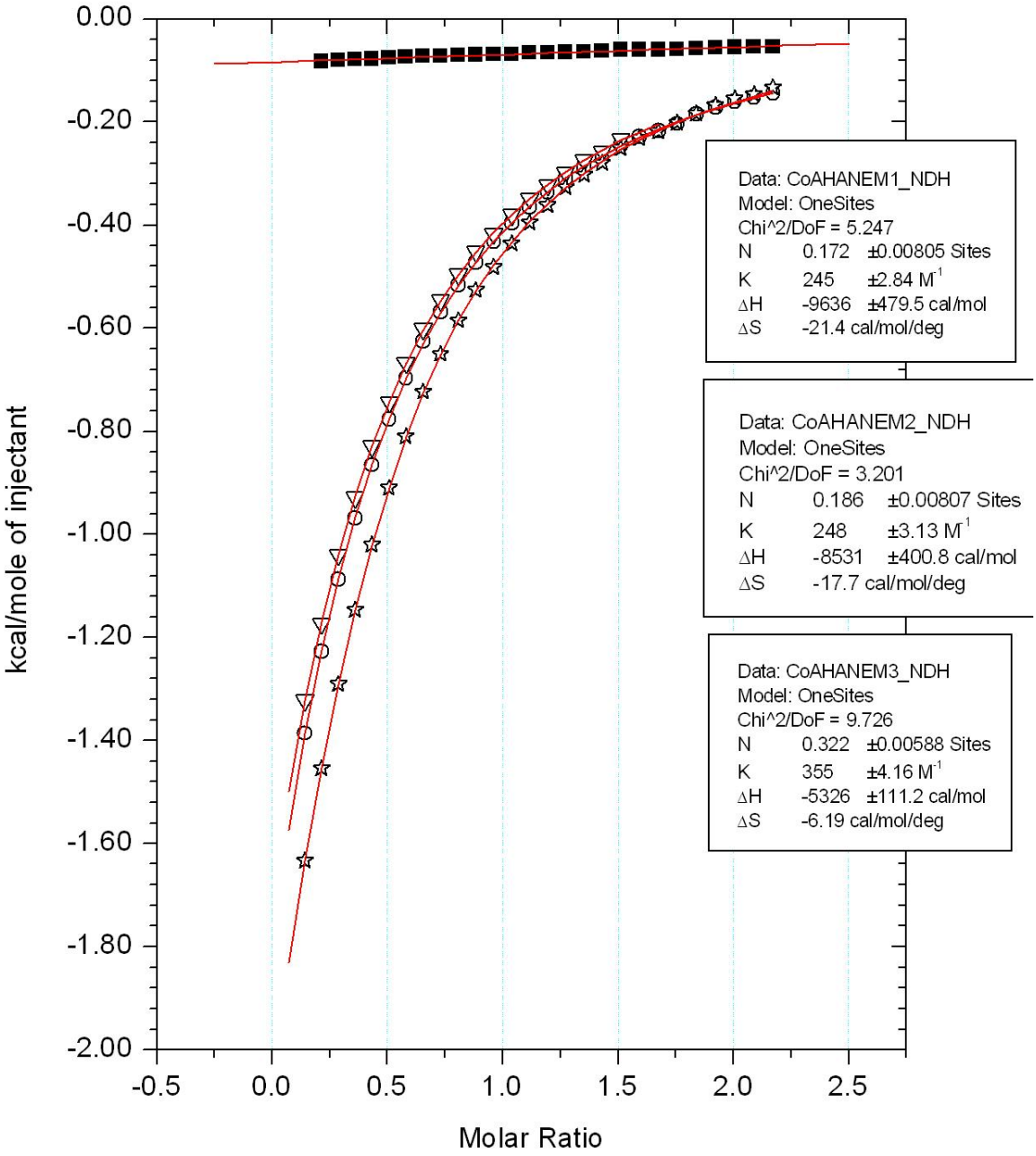

Figure 2.17: Fitting of Cobalt(II) into AHA isotherms. *An overlay of the three triplicate experiments of 50 mM $CoCl_2$ into 5 mM AHA is shown with the open symbols. The cobalt(II) control is shown with solid symbols. The control was subtracted from each isotherm before fitting the curve.*

2.7 Summary of Binding Parameters

A summary of the experimental conditions and average thermodynamic binding parameters is shown in Table 2.1. All errors are reported as standard deviations calculated from two, three, four or five trials. For experiments where there is no standard deviation reported for the n-values, it was fixed at the given number (typically 0.5) to yield the lowest reduced chi-squared for the curve.

Table 2.1: Summary of Run Conditions and Average Thermodynamic Binding Parameters.

Solvent Conditions	**Titrant**	**Titrate**	**Average Thermodynamic Binding Parameters**
60% anhydrous methanol and 40% 50 mM NEM, 150 mM NaCl buffer pH 6.80	10 mM SAHA	1 mM $ZnCl_2$	n = 0.50 (fixed) sites K= 4.3 ± 0.5 x10^2 M^{-1} ΔH= -8.0 ± 0.2 x10^3 cal/mol ΔS= -14.7 ± 0.6 cal/mol·deg ΔG°= -15.0 ± 0.3 kJ/mol
	20 mM SAHA	3 mM $CoCl_2$	n = 0.50 (fixed) sites K= 2.0 ± 0.5 x10^2 M^{-1} ΔH= -5.6 ± 0.7 x10^3 cal/mol ΔS= -8.5 ± 2.7 cal/ mol·deg ΔG°= -13.1 ± 0.7 kJ/mol
	20 mM AHA	2 mM $ZnCl_2$	n =0.52 ± 0.17 sites K= 4.4 ± 0.8 x10^2 M^{-1} ΔH= -8.6 ± 3.2 x10^3 cal/mol ΔS= -17± 11 cal/ mol·deg ΔG°= -15.0 ± 0.5 kJ/mol
	20 mM AHA	2 mM $CoCl_2$	n = 0.58 ± 0.12 sites K= 3.2 ± 0.4 x10^2 M^{-1} ΔH= -5.0 ± 1.2 x10^3 cal/mol ΔS= -5 ± 4 cal/ mol·deg ΔG°= -14.3 ± 0.4 kJ/mol
50 mM NEM, 150 mM NaCl buffer pH 6.80	50 mM AHA	5 mM $ZnCl_2$	n = 0.51 ± 0.06 sites K= 3.6 ± 0.4 x10^2 M^{-1} ΔH= -2.5 ± 0.2 x10^3 cal/mol ΔS= 3.2 ± 0.8 cal/ mol·deg ΔG°= -14.6 ± 0.3 kJ/mol
	100 mM AHA	10 mM $ZnCl_2$	n = 0.33 ± 0.06 sites K= 6.5 ± 0.2 x10^2 M^{-1} ΔH= -2.5 ± 0.2 x 10^3 cal/mol ΔS= 4.57± 0.69 cal/ mol·deg ΔG°= -16.1 ± 0.1 kJ/mol
	50 mM AHA	5 mM $CoCl_2$	n = 0.26 ± 0.01 sites K= 2.1 ± 0.3 x 10^2 M^{-1} ΔH= -7.2 ± 0.3 x10^3 cal/mol ΔS= -13.5± 1.0 cal/ mol·deg ΔG°= -13.2 ± 0.1
	50 mM $CoCl_2$	5 mM AHA	n = 0.23 ± 0.08 sites K= 2.8 ± 0.6 x 10^2 M^{-1} ΔH= -7.8 ± 2.2 x 10^3 cal/mol ΔS= -15.1 ± 7.9 cal/ mol·deg ΔG°= -13.9 ± 0.5 kJ/mol

N is the number stoichiometric binding sites on the titrant, K is the equilibrium binding constant, ΔH is the change in enthalpy and ΔS is the change in entropy and ΔG° is the change in Gibbs free energy.

Tables 2.2 and 2.3 show the parameters obtained under each solvent condition. These data were previously unavailable prior to this study. As stated earlier, the parameters obtained for AHA were used to determine if the thermodynamic parameters for SAHA could be extrapolated into aqueous conditions. Table 2.2 shows the parameters obtained for the interaction of AHA with zinc(II) and cobalt(II) as well as the interaction of SAHA with zinc(II) and cobalt(II) in the methanol: buffer mixture. Table 2.3 shows the parameters obtained for the interaction of AHA with zinc(II) and cobalt(II) in NEM buffer. Using the parameters and associated errors it can be seen that the values obtained in the two different solvents agree. These conclusions are what allow the interactions with SAHA with the metal ions in NEM buffer to be extrapolated. Based on this, the parameters obtained for the interaction of SAHA with zinc(II) and cobalt(II) in the methanol: buffer mixture are most likely within error of what they would be in buffer.

Table 2.2: Summary of Thermodynamic Binding Parameters Obtained in the 60% Methanol 40% Buffer Mixture.

Titrant	**Titrate**	**N (sites)**	**K (M^{-1})**	**ΔH (cal/mol)**	**ΔS (cal/mol·deg)**	**ΔG° (kJ/ mol)**
SAHA	Zn	0.5 (fixed)*	$4.3 \pm 0.5 \times 10^2$	$-8.0 \pm 0.2 \times 10^3$	-14.7 ± 0.6	-15.0 ± 0.3
	Co	0.5 (fixed)*	$2.0 \pm 0.5 \times 10^2$	$-5.6 \pm 0.7 \times 10^3$	-8.5 ± 2.7	-13.1 ± 0.7
AHA	Zn	0.52 ± 0.17	$4.4 \pm 0.8 \times 10^2$	$-8.6 \pm 3.2 \times 10^3$	-17 ± 11	-15.0 ± 0.5
	Co	0.58 ± 0.12	$3.2 \pm 0.4 \times 10^2$	$-5.0 \pm 1.2 \times 10^3$	-5 ± 4	-14.3 ± 0.4

*****Curve is not unique enough to yield a unique set of binding parameters

Table 2.3: Summary of Thermodynamic Binding Parameters Obtained in Buffer.

Titrant	**Titrate**	**N (sites)**	**K (M^{-1})**	**ΔH (cal/mol)**	**ΔS (cal/mol·deg)**	**ΔG° (kJ/ mol)**
AHA	Zn	0.51 ± 0.06	$3.4 \pm 0.4 \times 10^2$	$-2.5 \pm 0.2 \times 10^3$	3.2 ± 0.8	-14.6 ± 0.3
		0.33 ± 0.06	$6.5 \pm 0.2 \times 10^2$	$-2.5 \pm 0.2 \times 10^3$	4.6 ± 0.7	-16.1 ± 0.1
	Co	0.26 ± 0.01	$2.1 \pm 0.3 \times 10^2$	$-7.5 \pm 0.3 \times 10^3$	-13.5 ± 1.0	-13.2 ± 0.1
Co	AHA	0.23 ± 0.08	$2.8 \pm 0.6 \times 10^2$	$-7.8 \pm 2.2 \times 10^3$	-15.1 ± 7.9	-13.9 ± 0.5

2.8 Final Remarks

There were several problematic steps within this set of ITC experiments. First, the poor solubility of SAHA in aqueous solution forced us to turn to methanol as the solvent which is not a physiological solvent. The methanol: buffer mixture at pH 6.80 was a step closer towards a physiologically relevant condition and it effectively reduced the baseline noise, a problem that plagued the signals in titrations using 100% methanol. Other ratios of solvent mixtures were not examined in this work but the differences in the binding energetics obtained in the methanol: buffer mixture and in NEM buffer were insignificant. This suggests that slight variations in the solvent percentages do not make a significant contribution to the resulting parameters.

Another problem encountered was the effect of degassing samples prepared in methanol on data reproducibility. Degassing is normally necessary to remove trapped air, preventing heat spikes that can result from air bubbles as they get dislodged during a titration experiment. Degassing thus lowers the signal-to-noise level and increases accuracy of the resulting binding parameters. However, degassing became problematic for samples prepared in methanol or in the methanol: buffer mixture due to the volatile nature of methanol. Degassing significantly changes the composition of the solvent, i.e. the solvent is no longer 60% methanol and 40% buffer, and also changes the overall concentration of the solute by reducing the total volume. To avoid these complications, the samples prepared in the methanol: buffer mixture were not degassed. This proved to more than compensate for the disadvantage of an occasional air bubble due to not degassing.

Initially, we planned on examining the binding interaction of SAHA to zinc(II) and copper(II). The poor solubility of copper(II) also posed a challenge because copper(II) was not

soluble enough in NEM buffer or the mixture (both at pH 6.80) to yield the minimum concentration needed for the ITC experiments. Cobalt(II) ion was chosen instead. For the future, if the interaction of copper (II) with SAHA or other HDAC inhibitors is to be studied using ITC, different solvent ratios, different buffers and different pH values could be tested until a high enough solubility is reached.

The hygroscopic nature of AHA was also a problem. When a molecule is hygroscopic it immediately absorbs water from the air it is exposed to thereby altering the molecular formula weight of the compound. This makes it extremely difficult to mass out an accurate amount of AHA. To counteract this physical property of AHA, it was removed in small portions under nitrogen atmosphere and the bottles were then sealed to avoid air contact. When solutions were made, the solid was massed as quickly as possible to try to limit the amount of water absorbed by the compound. Once the bottle was opened and the required amount was removed for solution preparation, the remaining AHA in the bottle was discarded.

Another factor examined was the stability of SAHA and AHA under the chosen solvent conditions. Currently, the solution stability data of SAHA and AHA is not readily available. However, it is well known that the hydroxamic group is relatively unstable and the hydrolysis of this functional group results in a hydroxyl amine and a carboxylic acid. To ensure that the results obtained in these studies was a direct result of a binding interaction between AHA or SAHA and zinc(II) or cobalt(II), fresh solutions of AHA and SAHA were prepared and used no more than 25 minutes before beginning the titration experiment. This was done to ensure that the majority of the solution was composed of fully intact molecules. The additional runs obtained using fresh SAHA or AHA did not differ significantly from runs using much older solutions. This evidence implies that the binding curves obtained are a result of the binding interaction between the metal

and the hydroxamic acid group. The runs using freshly prepared solutions were incorporated when calculating the average binding parameters for each system. Additionally, titration experiments using a mixture of the hydrolysis products of AHA (hydroxyl amine and acetic acid) and zinc(II) or cobalt(II) were completed. The binding curves obtained from the runs using the hydrolysis products were compared to previous runs using AHA. These curves show that the degradation products of AHA look like control experiments with small heats of binding that are constant throughout the entire titration experiment. This implies that the binding isotherms are a result of a binding interaction between the metal ion and the intact AHA or SAHA molecules, not between the metal ion and the hydrolysis products or the heat related to the hydrolysis of AHA or SAHA (data not shown).

The quality of the data may be improved if the percentage of buffer in the solvent mixture was increased. This may allow for less baseline noise and the ability to obtain reproducible results easily. Additional experiments to determine the highest percentage of buffer (in a methanol:buffer mixture) that solubilizes SAHA would be beneficial knowledge, as the increased solubility of SAHA could allow for a more reliable binding curve. Currently the c-value is between 0.20 and 0.30 which is well outside of the desired range. This introduced significant error when determining the binding parameters because the resulting curves lack the unique characteristics to fit one set of parameters. Increasing the c-value to be within the 1-1000 range would increase the accuracy of the binding parameters extracted, especially the binding stoichiometry. However, a significant increase in SAHA solubility would need to occur in order to be within the desired range of c-values. The concentration within the cell would need to be 5 mM which means that the concentration of SAHA in the syringe would need to be approximately 50 mM. Currently, under the chosen solvent conditions the maximum solubility of SAHA is 20

mM. Perhaps exploring other buffers, a lower salt concentration or different pH would affect the solubility and allow SAHA to become more soluble thereby increasing the reliability of the binding parameters obtained.

Future directions of this project would be to express and purify an HDAC isoform in a high enough quantity that ITC experiments using the protein and SAHA could be done. This would be valuable data that could be used to directly determine the binding affinity of SAHA. Another future direction is to test other hydroxamic acid inhibitors of HDAC such as Trichostatin A (TSA) or using other analogs of SAHA to determine the variations in the binding energetics. These data would be valuable because no thermodynamic binding data is available for these types of inhibitors. The binding energetics data obtained would be invaluable to design better inhibitors en route to the development of anti-cancer therapeutics..

Chapter 3: Fluorogenic Assays of HDACs and Small Molecule NO Donor Inhibitors

To determine if HDAC8 is inhibited by the selected nitric oxide donors which covalently modify free cysteine residues on the solvent exposed surface, a discontinuous fluorogenic assay of HDAC8 was performed. A broad range inhibitor screen (10 and 100 μM) was done to determine if and at what potency the NO donors were inhibiting the enzyme. These determinations were based off a 7-amino-4-methylcoumarin (AMC) standard curve. Once screened, NO donors were selected based on their percent inhibition and a tighter range screening was conducted to try and determine the half maximal inhibitory concentration (IC_{50}) for the commercial NO donors. Additional screens of synthesized compounds, S-nitrosocysteine and ethanesulfohydroxamic acid as well as commercially available SAHA and AHA were performed. Overall only SAHA showed inhibitory effects on HDAC8.

3.1 Constructing an AMC Standard Curve

The deacetylation assay of HDAC8 produces the fluorescent molecule 7-amino-4-methylcoumarin (AMC), after deacetylation and subsequent cleavage by the developer. The chemical structure of AMC is shown in Figure 3.1. We can accurately determine the concentration of AMC produced during a reaction because the concentration is relative to the RFUs (relative fluorescent units). The RFUs are dependent upon the settings of individual instruments deeming it necessary to prepare our own standard curve. The equation of the line, $y = 0.00015x + 0.113$, for the standard curve of RFUs versus the concentration of AMC was used to calculate the amount of AMC produced once HDAC8 was exposed to the NO donors. The standard curve, represented in Figure 3.2, contains concentrations ranging between 0 and 10 μM. This is sufficient to cover the experimental assays. Even though each well had 25 μM

AMC-containing substrate, significantly less free AMC was produced (< 10 µM) after reaction with HDAC8.

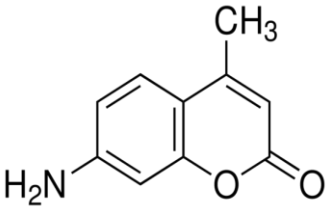

Figure 3.1: Chemical Structure of AMC.

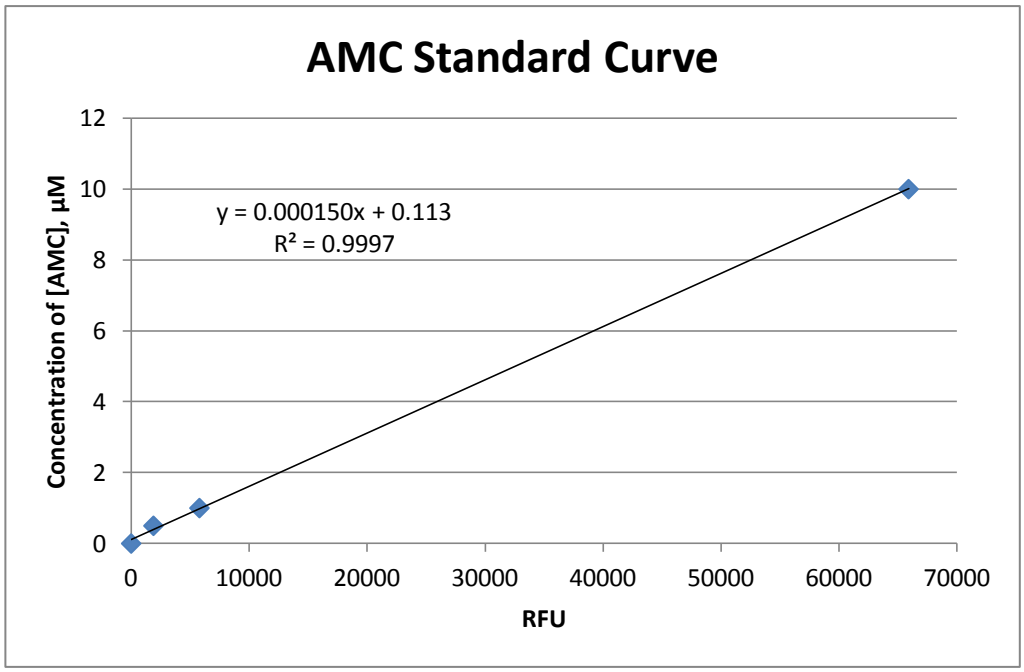

Figure 3.1: AMC Standard Curve. *The points on the curve represent 0, 0.5, 1 and 10 µM AMC in DMSO in the HDAC8 assay buffer at pH 8.0. The linear trend line of y=0.000150x+ 0.113 is reliable as determined by the R^2 value close to 1.0 implying a linear fit.*

3.2 Screening Nitric Oxide Donors

In order to determine if any of the commercially available nitric oxide donors are possible inhibitors of HDAC8 a broad concentration assay using inhibitor concentrations of 100 µM and 10 µM was completed. Table 3.1 shows the results which include the concentration of AMC produced during the assay and the percent activity of HDAC remaining as compared to the control HDAC8 reaction.

Table 3.1: Broad Range Inhibition Screen of Commercial NO Donors.

Inhibitor 100 µM	RFUs	[AMC] µM	% Activity	Inhibitor, 10 µM	RFUs	[AMC] µM	% Activity
SNAP	3062	0.7254	81	SNAP	2677	0.6484	72
SNP	2467	0.6064	67	SNP	2813	0.6756	75
DEA	2851	0.6832	76	DEA	2345	0.5820	**65**
JS-K	2365	0.5860	**65**	JS-K	3612	0.8354	93
Control	3932	0.8994	100				

Screening performed using 400 nM HDAC8 in each well.

Based on the data in Table 3.1, the inhibitors that resulted in the lowest percent activity of HDAC8, or the greatest amount of enzymatic inhibition, were 10 µM DEA and 100 µM JS-K both with percent activities of 65%. Therefore, a smaller range of concentrations for these two inhibitors were screened with the goal of determining the IC_{50} for each inhibitor. More detailed screens of SNP and SNAP were performed because they are well known nitric oxide donors that inhibit a variety of enzymes. An additional assay using the NO-donor S-nitrosocysteine was also performed. Figure 3.3 shows the results of the more detailed screen using JS-K. At the high concentrations of 150 and 125 µM, a small extent of inhibition occurred, as observed though the percent activities of 86% and 63%, respectively. These are extremely high concentrations and are not considered relevant in drug discovery as typically, to be considered a potential drug candidate the potency must be below 10 µM. Figure 3.4 shows that DEA NONOate activated rather than inhibited HDAC8. This is evident though the percent activities ranging from 105% to

153%. These results suggest that the screens performed (Table 3.1) were not reliable because they were not performed in replicate.

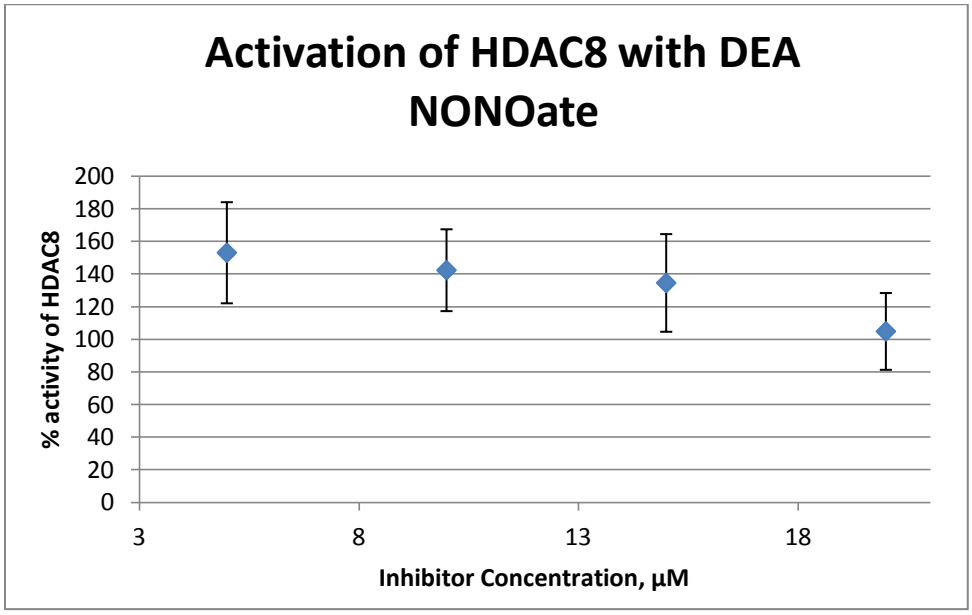

Figure 3.3: Activation of HDAC8 with DEA NONOate. *A plot of inhibitor concentration versus the percent HDAC8 activity remaining relative to a DMSO control. Varying concentrations of DEA NONOate between 20 µM and 5 µM and 400 nM HDAC8 were screened in triplicate. The RFUs measured were averaged. Error bars are calculated using root mean square error.*

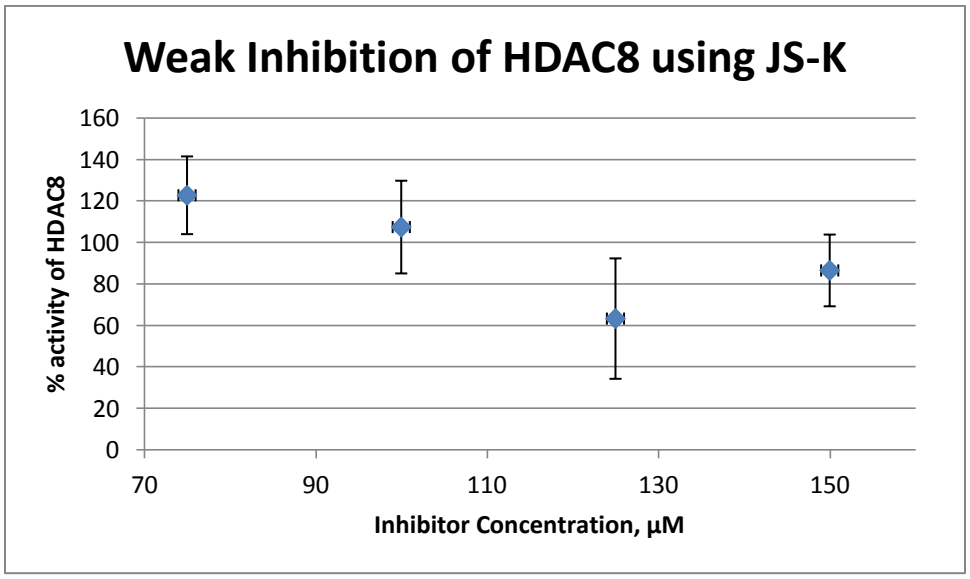

Figure 3.4: Weak Inhibition of HDAC8 using JS-K. *A plot of inhibitor concentration versus the percent HDAC8 activity remaining relative to a DMSO control. Varying concentrations of JS-K between 150 µM and 75 µM and 400 nM HDAC8 were screened in triplicate. The RFUs were measured and averaged. Error bars are calculated using root mean square error.*

The assays in Figures 3.3 and 3.4 were performed using 400 nM HDAC8 which is very high for medium-to-high throughput 96-well plate assays. To optimize the assay conditions and conserve enzyme, a control assay of HDAC8 using varying concentrations between 25 and 400 nM was conducted to determine the lowest concentration of HDAC8 required for visible activity. Table 3.2 shows that the enzyme at all concentrations used were visibly active. Thus, the concentration of HDAC was reduced to 25 nM for subsequent assays to conserve enzyme. However, in the presence of the lower concentration of HDAC, the NO donors still yielded significant activation rather than inhibition as shown in Figure 3.5.

Table 3.2: Optimization of HDAC8 Concentration.

[HDAC8](nM)	RFUs	[AMC] (µM)
400	2216	0.556
333	1405	0.394
166	1043	0.322
83.6	947	0.302
41.8	863	0.286
25	852	0.283

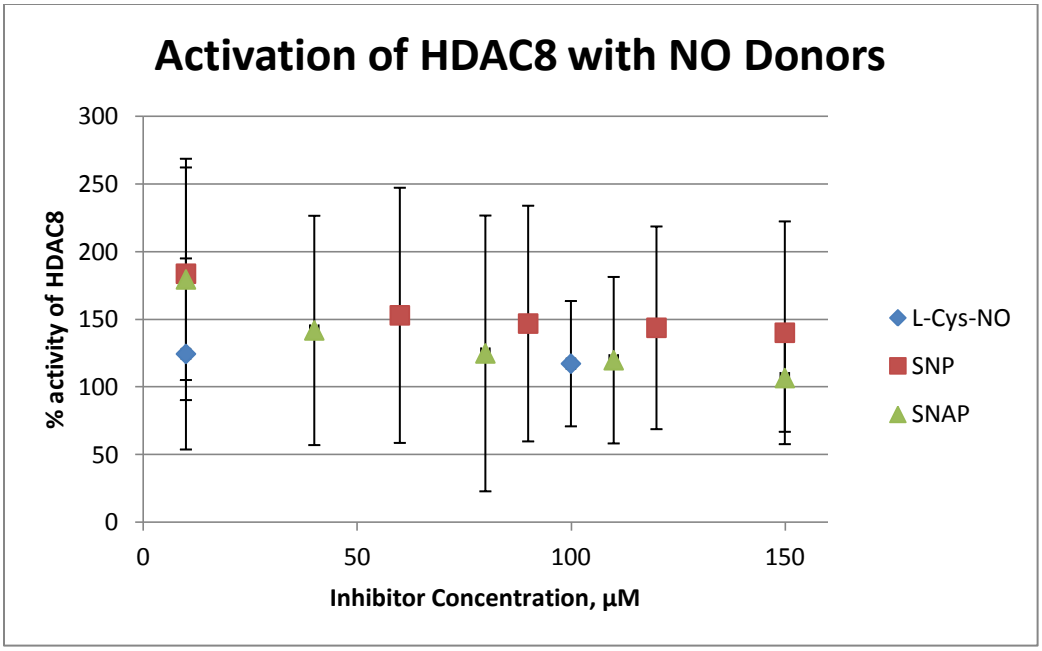

Figure 3.5: Activation of HDAC8 with Nitric Oxide Donors. *A plot of inhibitor concentration versus the percent activity of HDAC8 relative to a DMSO control. Varying concentrations of a nitric oxide donor inhibitor in µM were incubated with 25 nM HDAC8 and the fluorescence in RFUs of the triplicate wells were averaged. Inhibitor abbreviations are as follows: S-nitrosocystene (L-Cys-NO), Sodium nitroprusside (SNP), and S-nitroso-N-acetyl-penacillamine (SNAP). Error bars were calculated using root mean square error.*

The results in Figure 3.5 were suspicious because these are all well known NO donors that were expected to show slight inhibition. The large error bars shown in Figure 3.5 indicate that the results are unreliable because most points have error bars ranging from as low at 50% activity all the way up to 250% activity. This large range does not allow us to conclusively comment on the effectiveness of the inhibitors. To verify these results, a repeat screening of SNP was conducted. This assay yielded even higher percent errors suggesting there was a flaw in the assay itself. Therefore, two controls were performed; one using the normal incubation procedure of HDAC8 and inhibitor at room temperature and the other on ice. The results of this assay showed that there were no differences in the observed RFUs between the two controls suggesting that the incubation at room temperature was not the issue. (results not shown). An additional control assay was conducted to determine the background fluorescence of HDAC8. This assay

showed that the enzyme had slight fluorescence but not a significant amount (results not shown). Based on these data it was concluded the HDAC8 activity was too low to accurately monitor the activity; suggesting the enzyme may have become inactivated due to multiple freeze and thaw cycles.

Using a newly acquired enzyme sample, a repeat screen of SNP using 25 nM HDAC was conducted. Table 3.3 shows the data obtained using concentrations of SNP between 150 µM and 10 µM with 25 nM HDAC8. Again, no inhibitory activity was observed which is evident from the data in Table 3.3 which shows that the lowest percent activity value was 97%. In combination with the initial broad screening results, this suggests that an increased concentration of HDAC is required to reproducibly visualize enzymatic activity.

Table 3.3: SNP Assay Using New HDAC8.

[Inhibitor] (µM)	RFUs	[AMC] (µM)	% activity
0	159	0.145	100 ± 27
150	142	0.142	98 ± 22
110	135	0.140	97 ± 24
80	155	0.144	99 ± 22
40	157	0.144	100 ± 28
10	139	0.141	97 ± 19

Assay was set up using 25 nM HDAC8. Error is reported as root mean square error.

At low enzyme concentration with the same amount of substrate (25 µM), the enzyme is in the presence of a higher ratio of substrate than if an optimized concentration of HDAC8 (400 nM) was used. Because the IC_{50} values are unknown, it is beneficial to prevent flooding the enzyme with substrate by having a greater ratio of enzyme to substrate; if the enzyme is saturated with substrate then the likelihood of inhibition decreases because the enzyme is going to act on the substrate (which is present in higher concentration) than the NO donor. Thus, the concentration of HDAC8 was increased to 100 nM to ensure that the ratio of enzyme to substrate was higher. In addition, because SNP, JS-K and DEA NONOate did not show evidence of significant inhibition, additional NO donor functional groups were tested. A known inhibitor of

HDAC, suberoylanilide hydroxamic acid, or SAHA, a small molecule hydroxamic acid acetohydroxamic acid, or AHA, SNAP and L-CysNO were used in this screening. Table 3.4 shows the results of these screens. Despite the use of a higher concentration of enzyme no significant inhibition was observed. Table 3.4 shows that even SAHA, a potent, known inhibitor of HDACs showed only slight inhibition, as evidence by the percent activities ranging from 83% to 104%. Additionally, the percent activities for AHA ranged from 90% all the way up to 115% and L-CysNO had percent activities ranging from 90% to 103%.

Table 3.4: SAHA, AHA, and SNP Screening.

	[Inhibitor] (µM)	Average RFUs	[AMC] (µM)	% Activity
Control	0	898	0.293	100 ± 23
SAHA	150	643	0.242	83 ± 14
	110	810	0.275	94 ± 38
	80	869	0.287	98 ± 29
	40	955	0.304	104 ± 76
	10	815	0.276	94 ± 29
AHA	150	1070	0.327	112 ± 29
	110	1110	0.335	115 ± 20
	80	787	0.270	92 ± 58
	40	1023	0.318	108 ± 23
	10	746	0.262	90 ± 28
SNAP	150	766	0.266	91 ± 23
	110	804	0.274	94 ± 23
	80	938	0.301	103 ± 36
	40	753	0.264	90 ± 23
	10	824	0.278	95 ± 29

Data collected using 100 nM HDAC8 enzyme. Reported error values are shown as root mean square error.

It is hypothesized that the absence of inhibition observed in previous assays was a consequence of using too low an enzyme concentration. Thus, the results obtained from the assays using concentrations of enzyme other than 400 nM are unreliable. Once the concentration of HDAC was increased to the originally tested concentration 400 nM, L-CysNO, SNAP and ESHA, a sulfonyl derivative of a hydroxamic acid yielded inconclusive evidence on whether or not inhibition was occurring due to large percent errors. However, SAHA, which has been

shown to act as both a competitive active site inhibitor as well as an NO donor upon oxidation in the body, showed strong evidence of inhibition as the percent activity using only 40 μM SAHA was 35% (Table 3.5) This could be indirect evidence supporting a dual inhibitory mechanism through active site competitive inhibition and release of nitric oxide. [35] However, these studies did not determine how much inhibition is caused by competitive inhibition and how much is caused by the release of NO. The percent activities observed using SNAP, L-CysNO, and ESHA at 400 nM enzyme seems to be suggest that the interaction of these small molecule inhibitors is weak under the chosen assay conditions as evidence by the minimal decreases in percent activity as well as the large associated errors.

Table 3.5: SAHA, ESHA, L-CysNO and SNAP Screening.

	[Inhibitor] (μM)	RFUs	[AMC] (μM)	% activity
Control	0	2053	0.0464	100 ± 10
SAHA	150	588	0.0133	29 ± 4
	110	616	0.0139	30 ± 3
	80	875	0.0198	43 ± 17
	40	727	0.0164	35 ± 3
SNAP	150	2225	0.0503	108 ± 7
	110	2282	0.0516	111 ± 8
	80	2162	0.0489	105 ± 12
	40	1922	0.0434	94 ± 9
L-CysNO	150	1932	0.0437	94 ± 6
	110	1852	0.0418	90 ± 13
	80	2379	0.0538	116 ± 12
	40	2096	0.0474	102 ± 11
ESHA	150	1347	0.0304	66± 38
	110	1487	0.0336	72 ± 28
	80	1436	0.0325	70 ± 20
	40	2659	0.0601	130 ± 38

Data collected using 400 nM HDAC8. The error is reported as a root mean square error percentage.

3.3 Final Remarks

Overall, this study shows that the commercially available NO donors tested did not inhibit HDAC8 under the chosen assay conditions. Suberoylanilide hydroxamic acid, a positive control due to the fact that it is a known HDAC inhibitor, did inhibit strongly. This is

exemplified by the percent activities of HDAC8 ranging between 29% and 43%. Figure 3.6 shows the surface structure of HDAC8. There are 10 cysteine residues present in the protein with 3 exposed to the surface. None of the cysteines are involved in disulfide bonds. In addition, Figure 3.6 shows that most of them are buried within the protein and are not accessible to the solvent and therefore not accessible to nitric oxide. Nitric oxide inhibition occurs through covalent modification of solvent exposed free sulfhydryl groups on cysteine residues. The low number of solvent exposed cysteine residues could be the main explanation of why only the hydroxamic acid and sulfonyl derivative showed any inhibition.

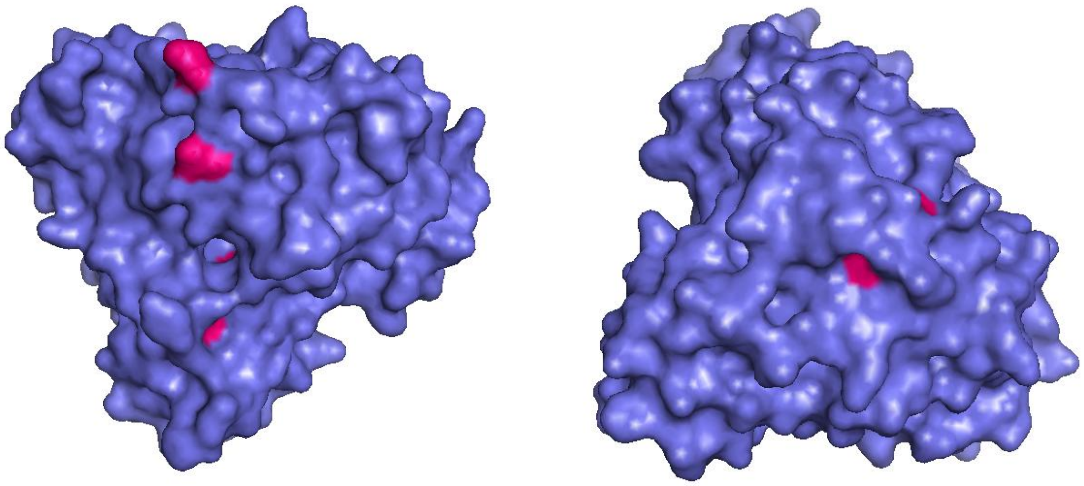

Figure 3.6: Surface Structure of HDAC8 with Labeled Cysteine Residues. *Figure of surface diagram of PDB structure 1T69 visualized using Pymol. Structure on left and right are a 180° rotation of each other.*

In future studies, the assay could be further optimized using a lower concentration of both substrate and enzyme to lower the overall cost of the assay. Furthermore, a reducing agent such as dithiothreitol (DTT) or tris(carboxyethyl) phosphine (TCEP) could be added to the reaction mixture. This would be useful because while there are no structural disulfide bonds present in the protein, disulfides readily form in air under oxidizing conditions when cysteine residues are close enough in space making them much more stable. By adding the reducing agent to the mixture it

would prevent the cysteine residues that are exposed to the surface from being oxidized into disulfide bonds. Screening of additional NO donor compounds such as a known effective NO donor for histone deacetylases, GSNO, could be done to determine its inhibitory strength. Overall the development of a new assay for HDACs that is continuous and does not use a cysteine protease would be extremely beneficial to furthering assays using HDACs. The assay we used likely contains a cysteine protease because it cleaves after lysine residues in the substrate. The use of a cysteine containing protease is going to affect the assay because it contains an extremely reactive cysteine so the NO donor will likely act on that reactive cysteine as opposed to the cysteine residues in HDAC8.

Chapter 4:
Experimental Methods

4.1 Isothermal Titration Calorimetry

a. General Considerations

Stock solutions of each component (SAHA, AHA, $ZnCl_2$ and $CoCl_2$) were prepared using stoichiometric calculations to determine the grams required to prepare the solution. All solutions were prepared using the highest grade of purity reagents available. The transition metals zinc(II) (II) chloride, 99.99%, extra pure was purchased from Acros Organics and cobalt(II) (II) chloride, 98%, ACS reagent was purchased from Sigma-Aldrich. The HDAC inhibitor suberoylanilide hydroxamic acid was purchased from Fischer Scientific. Acetohydroxamic acid, 98+% was purchased from Acros Organics. All reagents were massed on the Ohaus analytical standard balance. The pH meter was calibrated using buffer solutions at pH 4.00±0.01, 7.00±0.01, and 10.00±0.02 purchased from Fischer Scientific. The buffer was prepared using MilliQ water with a purity of $\leq$ 18 MΩ. The methanol: buffer mixture was prepared using 99.8% pure anhydrous methanol removed under nitrogen atmosphere. All solution pHs were corrected using the Orion pH meter (model 420A). The Rainin p1000, p200, p20 and p10 pipettemen were for removing small volumes. Stock solutions were prepared in 50 mL and 15 mL Fischer brand disposable centrifuge tubes. Stock solutions were mixed on the Maxi Mix II Thermolyne Type 37600 mixer. Samples were degassed using the Thermovac (GE, formerly MicroCal, Piscataway, NJ). All calorimetric measurements were carried out using a VP-ITC Isothermal Titration Calorimeter (GE, formerly MicroCal, Piscataway, NJ).

b. Solution Preparation

The solutions of metal ions and hydroxamic acids were prepared based on mass measurements determined by stoichiometric calculations. The metal ions are stable in solution thus fresh solutions were only prepared when previously prepared solutions ran out. However, fresh solutions of both copper and zinc(II) were prepared to determine if the results obtained differed with new solutions. The same principle remained true for AHA. However, since the solution stability of AHA is lower than the metal ions the fresh AHA solutions were prepared for one run for each system within 25 minutes of beginning the experiment. Stock solutions were diluted following the $M_1V_1 = M_2V_2$ to prepared the necessary concentrations for each experiment.

c. Experimental Procedure

Prior to titration, the samples were usually degassed for 5 minutes to remove air bubbles that otherwise can get dislodged during the experiment, generating unwanted heat. When methanol or methanol: buffer mixture was used, samples were not degassed to avoid changes in solvent composition and solute concentration. A 250-µL injection syringe was filled with the titrant and the 1.4 mL reaction cell was filled with titrate. The reference cell was filled with buffer or solvent depending on the experiment. A typical experiment involved 28 injections of titrant of 10 µL each into the reaction cell. Each injection lasted 20 seconds and injections were spaced 250 or 300 seconds apart. The syringe was rotated at 307 rpm and the cell temperature was calibrated to 25°C.

For most ITC experiments, the transition metal solutions of either zinc(II) or cobalt(II) were loaded into the sample cell and SAHA or AHA was loaded into the syringe and inserted

into the sample cell. Concentrations of titrant and titrate for the different experiments varied (Table 1) while the basic experimental parameters of number of injections, injection volume, injection duration, and spacing remained the same through the experiments. Control titrations were performed by titrating titrant into solvent or buffer or titrating solvent or buffer into titrate. The heat data from these control titrations were later subtracted to remove heat effects due to processes other than titrant-titrate interaction. All titrations were repeated in triplicate to ensure that the results were reproducible.

Table 4.1*: *Concentrations of Titrant and Titrate.

Solvent	Compound	Titrant (mM)	Compound	Titrate (mM)
Methanol: Buffer	SAHA	10	Zn^{2+}	1
		20	Co^{2+}	3
	AHA	20	Zn^{2+}	2
		20	Co^{2+}	2
Buffer	AHA	50	Zn^{2+}	5
		50	Co^{2+}	5
		100	Zn^{2+}	10
	Co^{2+}	50	AHA	5

The 60:40 mixture is 60% anhydrous methanol and 40% buffer (50 mM NEM, 150 mM NaCl buffer pH 6.80). The final pH of the mixture was 6.80. The buffer is 50 mM NEM, 150 mM NaCl buffer pH 6.80.

d. Data Analysis Procedures

Analysis of calorimetric data was carried out using the Origin 7.0 software. Data were fit to a one set of sites binding model using a nonlinear least square approach (Levenberg-Marquardt algorithm). This program package uses the heats generated for each injection and integrates the area under or above the curve to determine binding parameters including: n (the number titrant of binding sites on the titrate), K_a (the equilibrium binding constant), ΔH (the enthalpy change per mole of titrant), and ΔS (entropy change per mole of titrant). The $\Delta G°$ (the Gibb's free energy change per mole of titrant) can be calculated using the K_a.

The process of fitting experimental data to a binding model involves the following steps: manual correction of the baseline in the raw data plots to ensure that the baseline represents the data correctly, subtraction from the binding isotherm an average of control isotherms, fit the data to the one set of sites binding model to determine the binding parameters and view the fit to determine if it fits the curve well. We often find it necessary to subtract an additional constant equaling the plateau heat of the isotherm to minimize the value for Chi-squared. This likely reflects the fact that the control titration isn't a perfect control for the real control heat resulting from the processes other than binding, such as dilution of the titrant and titrate upon titration. The fitting parameters obtained after these manipulations were taken as the final binding parameters for each experiment. This process was repeated for each titration experiment and the parameters obtained were averaged and a standard deviation was calculated for each system.

4.2 HDAC8 Fluorogenic Assays

a. General Considerations

Stock solution in dimethyl sulfoxide of each nitric oxide donor were prepared at 50 mM , 500 µM and 50 µM using stoichiometric calculations to determine the mass required of each component. All solutions were prepared using the reagents purchased from Sigma Aldrich at the highest purity available. The nitric oxide donors sodium nitrite, ≥ 98.0%, sodium nitroprusside dehydrate, ≥ 98.0%, JS-K, ≥ 97%, Diethylamine NONOate sodium salt hydrate, S-nitroso-N-acetyl-DL-penicillamine, ≥ 97.0%, Diethylenetriamine/nitric oxide adduct, ≥ 97.0% and L-Cysteine, ≥ 97% were used as received. All NO donor solutions were prepared in DMSO (Sigma Aldrich, ≥ 99.6%) and then diluted except DETA NONOate which was prepared in MilliQ water with a purity of ≤ 18 MΩ. The Fluor de Lys HDAC8 substrate and developer were purchased from Enzo Life Sciences and were used as received. The HDAC8 assay buffer was prepared

using reagents from Sigma Aldrich. The assay buffer was composed of 50 mM Trizma base(≥ 99.9%), 137 mM NaCl (≥ 99.0%), 2.7 mM KCl, (≥ 99.0%) and 1 mM $MgCl_2$ (≥ 98.0%). The pH of the buffer was corrected to 8.0 using a Fischer Scientific Accumet Basic AB15 pH meter. The pH meter was calibrated using buffer solutions at pH 4.00±0.01, 7.00±0.01, and 10.00±0.02 purchased from Fischer Scientific. All small volume pipetting for the assays were carried out using Eppendorf pipettmen. Stock solutions were prepared in 1.5 mL and 0.5 mL microcentrifuge tubes. Solutions were mixed using the Fischer Scientific Vortex Mixer. The microtitrate plate was read on the LBioTech Synergy H1 Hybrid Reader visualized using the Gen5 2.00 software . All data obtained was analyzed using Microsoft Excel 2007. All enzyme assays were performed in triplicate in 96 well plate format and the average values were used for analysis.

b. Assay Procedures

To begin, 15 µL HDAC8 enzyme (≥ 90.0% Sigma Aldrich) at 400 nM (some assays using 100 or 25 nM) was incubated for 30 minutes with 10 µL the required concentration of nitric oxide donor. Additionally, a DMSO control containing no nitric oxide donor was performed for each assay. After the incubation, 25 µL of 50 µM Fluor de Lys substrate was added and allowed to react for 30 minutes. Finally, 50 µL of 1X Fluor de Lys Developer was added and incubated for 1 hour. After the incubation, the microtitrate plate was read at 360 and 480 nm (the optimum wavelengths for coumarin fluorescence)

c. 4-Amino-7-methylcoumarin (AMC) Standard Curve

A standard curve plotted using the concentration of AMC versus the relative fluorescence units was constructed. The volume of DMSO did not exceed 10% of the 50 µL total reaction

volume. Using a 100 mM stock of AMC in DMSO, serial dilutions of 10 mM, 1 mM and 0.1 mM were prepared. Concentrations of AMC between 500 nM and 100 µM were prepared in the wells using the AMC stocks, DMSO and assay buffer as shown in Table 4.1. The plate was read at 380 and 460 nm.

Table 4.2: Sample Components for AMC Standard Curve.

[AMC]	Volume AMC (µL)	Volume DMSO (µL)	Volume Buffer (µL)
0	0	5	45
500 nM	2.5 of 10 µM	2.5	45
1 µM	0.5 of 100 µM	4.5	45
10 µM	0.5 of 1 mM	4.5	45
25 µM	1.25 of 1 mM	3.75	45
50 µM	2.5 of 1 mM	2.5	45
100 µM	0.5 of 10 mM	4.5	45

d. Preparation of S-nitrosocysteine

In a microfuge tube, 0.05 mmol L-cysteine was dissolved in 1.0 mL of 0.5 N HCl. Once dissolved, 0.5 mmol sodium nitrite was also dissolved in the solution. The pH of solution was adjusted to neutral using 1.0 M NaOH. Once prepared, the stock solution was diluted to 500 µM and 50 µM in DMSO.

e. Preparation of Ethanesulfohydroxamic acid

Ethanesulfohydroxamic acid was prepared in the Karver lab according to literature procedures. [32]

Chapter 5:
Bibliography

1. Zhang, Y.; Fang, H.; Jiao, J.; Xu, W., The structure and function of histone deacetylases: the target for anti-cancer therapy. *Curr Med Chem* **2008,** *15* (27), 2840-9.

2. Khare, S. P.; Habib, F.; Sharma, R.; Gadewal, N.; Gupta, S.; Galande, S., HIstome--a relational knowledgebase of human histone proteins and histone modifying enzymes. *Nucleic Acids Res* **2012,** *40* (Database issue), D337-42.

3. Rekowski, M. W.; Giannis, A., Histone acetylation modulation by small molecules: a chemical approach. *Biochim Biophys Acta* **2010,** *1799* (10-12), 760-7.

4. Ng, H. H.; Bird, A., Histone deacetylases: silencers for hire. *Trends Biochem Sci* **2000,** *25* (3), 121-6.

5. Finnin, M. S.; Donigian, J. R.; Cohen, A.; Richon, V. M.; Rifkind, R. A.; Marks, P. A.; Breslow, R.; Pavletich, N. P., Structures of a histone deacetylase homologue bound to the TSA and SAHA inhibitors. *Nature* **1999,** *401* (6749), 188-93.

6. Martin, M.; Kettmann, R.; Dequiedt, F., Class IIa histone deacetylases: regulating the regulators. *Oncogene* **2007,** *26* (37), 5450-67.

7. McKinsey, T. A.; Zhang, C. L.; Olson, E. N., Activation of the myocyte enhancer factor-2 transcription factor by calcium/calmodulin-dependent protein kinase-stimulated binding of 14-3-3 to histone deacetylase 5. *Proc Natl Acad Sci U S A* **2000,** *97* (26), 14400-5.

8. Dequiedt, F.; Van Lint, J.; Lecomte, E.; Van Duppen, V.; Seufferlein, T.; Vandenheede, J. R.; Wattiez, R.; Kettmann, R., Phosphorylation of histone deacetylase 7 by protein kinase D mediates T cell receptor-induced Nur77 expression and apoptosis. *J Exp Med* **2005,** *201* (5), 793-804.

9. Chang, S.; Bezprozvannaya, S.; Li, S.; Olson, E. N., An expression screen reveals modulators of class II histone deacetylase phosphorylation. *Proc Natl Acad Sci U S A* **2005,** *102* (23), 8120-5.

10. Berdeaux, R.; Goebel, N.; Banaszynski, L.; Takemori, H.; Wandless, T.; Shelton, G. D.; Montminy, M., SIK1 is a class II HDAC kinase that promotes survival of skeletal myocytes. *Nat Med* **2007,** *13* (5), 597-603.

11. Grozinger, C. M.; Schreiber, S. L., Regulation of histone deacetylase 4 and 5 and transcriptional activity by 14-3-3-dependent cellular localization. *Proc Natl Acad Sci U S A* **2000,** *97* (14), 7835-40.

12. Khan, O.; La Thangue, N. B., HDAC inhibitors in cancer biology: emerging mechanisms and clinical applications. *Immunol Cell Biol* **2012,** *90* (1), 85-94.

13. Monneret, C., Histone deacetylase inhibitors. *Eur J Med Chem* **2005,** *40* (1), 1-13.

14. Butler, K. V.; He, R.; McLaughlin, K.; Vistoli, G.; Langley, B.; Kozikowski, A. P., Stereoselective HDAC inhibition from cysteine-derived zinc-binding groups. *ChemMedChem* **2009,** *4* (8), 1292-301.

15. Grant, S.; Easley, C.; Kirkpatrick, P., Vorinostat. *Nat Rev Drug Discov* **2007,** *6* (1), 21-2.

16. Singh, R. K.; Mandal, T.; Balasubramanian, N.; Cook, G.; Srivastava, D. K., Coumarin-suberoylanilide hydroxamic acid as a fluorescent probe for determining binding affinities and off-rates of histone deacetylase inhibitors. *Anal Biochem* **2011,** *408* (2), 309-15.

17. Falconer, R. J.; Collins, B. M., Survey of the year 2009: applications of isothermal titration calorimetry. *J Mol Recognit* **2011,** *24* (1), 1-16.

18. Lewis, E. A.; Murphy, K. P., Isothermal titration calorimetry. *Methods Mol Biol* **2005,** *305*, 1-16.

19. (a) ITC Data Analysis in Origin MicroCal: Piscataway, NJ, 1998; pp 75-76; (b) Pierce, M. M.; Raman, C. S.; Nall, B. T., Isothermal titration calorimetry of protein-protein interactions. *Methods* **1999,** *19* (2), 213-21.

20. Gantt, S. L.; Gattis, S. G.; Fierke, C. A., Catalytic activity and inhibition of human histone deacetylase 8 is dependent on the identity of the active site metal ion. *Biochemistry* **2006,** *45* (19), 6170-8.

21. Feng, J. H.; Jing, F. B.; Fang, H.; Gu, L. C.; Xu, W. F., Expression, purification, and S-nitrosylation of recombinant histone deacetylase 8 in Escherichia coli. *Biosci Trends* **2011,** *5* (1), 17-22.

22. Chabane, N.; Zayed, N.; Afif, H.; Mfuna-Endam, L.; Benderdour, M.; Boileau, C.; Martel-Pelletier, J.; Pelletier, J. P.; Duval, N.; Fahmi, H., Histone deacetylase inhibitors suppress interleukin-1beta-induced nitric oxide and prostaglandin E2 production in human chondrocytes. *Osteoarthritis Cartilage* **2008,** *16* (10), 1267-74.

23. Kostourou, V.; Cartwright, J. E.; Johnstone, A. P.; Boult, J. K.; Cullis, E. R.; Whitley, G.; Robinson, S. P., The role of tumour-derived iNOS in tumour progression and angiogenesis. *Br J Cancer* **2011,** *104* (1), 83-90.

24. Postovit, L. M.; Sullivan, R.; Adams, M. A.; Graham, C. H., Nitric oxide signalling and cellular adaptations to changes in oxygenation. *Toxicology* **2005,** *208* (2), 235-48.

25. Larsen, L.; Tonnesen, M.; Ronn, S. G.; Storling, J.; Jorgensen, S.; Mascagni, P.; Dinarello, C. A.; Billestrup, N.; Mandrup-Poulsen, T., Inhibition of histone deacetylases prevents cytokine-induced toxicity in beta cells. *Diabetologia* **2007,** *50* (4), 779-89.

26. Nott, A.; Watson, P. M.; Robinson, J. D.; Crepaldi, L.; Riccio, A., S-Nitrosylation of histone deacetylase 2 induces chromatin remodelling in neurons. *Nature* **2008,** *455* (7211), 411-5.

27. Feelisch, M., The use of nitric oxide donors in pharmacolgical studies *Nanuyn-Schmiedeberg's Archives of Pharmacology* **1998,** *338* (1), 113-122.

28. Low, S. Y., Application of pharmaceuticals to nitric oxide. *Mol Aspects Med* **2005,** *26* (1-2), 97-138.

29. Nath, N.; Chattopadhyay, M.; Pospishil, L.; Cieciura, L. Z.; Goswami, S.; Kodela, R.; Saavedra, J. E.; Keefer, L. K.; Kashfi, K., JS-K, a nitric oxide-releasing prodrug, modulates ss-catenin/TCF signaling in leukemic Jurkat cells: evidence of an S-nitrosylated mechanism. *Biochem Pharmacol* **2010,** *80* (11), 1641-9.

30. Shinoda, J.; Whittle, I. R., Nitric oxide and glioma: a target for novel therapy? *Br J Neurosurg* **2001,** *15* (3), 213-20.

31. Belch, J. J.; Ho, M., Pharmacotherapy of Raynaud's phenomenon. *Drugs* **1996,** *52* (5), 682-95.

32. Huang, Z.; Velazquez, C. A.; Abdellatif, K. R.; Chowdhury, M. A.; Reisz, J. A.; DuMond, J. F.; King, S. B.; Knaus, E. E., Ethanesulfohydroxamic acid ester prodrugs of nonsteroidal anti-inflammatory drugs (NSAIDs): synthesis, nitric oxide and nitroxyl release, cyclooxygenase inhibition, anti-inflammatory, and ulcerogenicity index studies. *J Med Chem* **2011,** *54* (5), 1356-64.

33. Miller, M. R.; Megson, I. L., Recent developments in nitric oxide donor drugs. *Br J Pharmacol* **2007,** *151* (3), 305-21.

34. Watson, P. M.; Riccio, A., Nitric oxide and histone deacetylases: A new relationship between old molecules. *Commun Integr Biol* **2009,** *2* (1), 11-3.

35. Samuni, Y.; Flores-Santana, W.; Krishna, M. C.; Mitchell, J. B.; Wink, D. A., The inhibitors of histone deacetylase suberoylanilide hydroxamate and trichostatin A release nitric oxide upon oxidation. *Free Radic Biol Med* **2009,** *47* (4), 419-23.

36. Reymond, J. L.; Fluxa, V. S.; Maillard, N., Enzyme assays. *Chem Commun (Camb)* **2009,** (1), 34-46.

37. Maggiora, L. L.; Smith, C. W.; Zhang, Z. Y., A general method for the preparation of internally quenched fluorogenic protease substrates using solid-phase peptide synthesis. *J Med Chem* **1992,** *35* (21), 3727-30.

38. HDAC8 Fluorimetric Drug Discovery Kit- BML-AK518-A Fluor de Lys Fluorescent Assay System Enzo Life Sciences: pp 2-7.

39. Caymen Chemical SAHA Product Information (accessed May 21).

40. Pang, Y. P. Y., J.E., Proton Dissociation Energies of Zinc-Coordinated Hydroxamic Acids and Their Relative

Affinities for Zinc: Insight into Design of Inhibitors of Zinc-Containing Proteinases. *J. Phys. Chem. B* **2000,** *104* (27), 6499-6505.

41. The Chemistry of Hydroxylamines, Oximes and Hydroxamic Acids Rappoport, Z., Ed. John Wiley & Sons Ltd. : 2009. (accessed May 21, 2012).